KINETICS OF DISCONTINUOUS PRECIPITATION OF LIQUID PHASE IN CU-IN ALLOYS

By

Satish Kumar Gautam

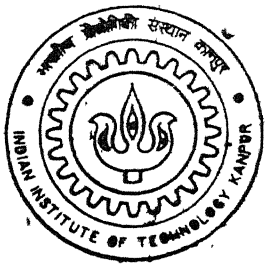

DEPARTMENT OF MATERIALS AND METALLURGICAL ENGINEERING

Indian Institute of Technology Kanpur

APRIL, 2002

KINETICS OF DISCONTINUOUS PRECIPITATION OF LIQUID PHASE IN CU-IN ALLOYS

A Thesis Submitted

in partial Fulfillment of the Requirements

for the Degree of

MASTER OF TECHNOLOGY

by

SATISH KUMAR GAUTAM

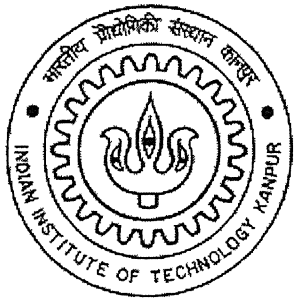

to the

DEPARTMENT OF MATERIALS AND METALLURGICAL ENGINEERING

INDIAN INSTITUTE OF TECHNOLOGY, KANPUR

APRIL, 2002

Dedicated to

My parents and family members.

CERTIFICATE

This is to certify that the work contained in the thesis entitled "**Kinetics of Discontinuous Precipitation of Liquid Phase in Cu-In Alloys**" by Mr. Satish Kumar Gautam has been carried out under my guidance and that this work has not been submitted elsewhere for a degree.

Dr. S.P.Gupta
Department of Materials and Metallurgical Engineering,
Indian Institute of Technology,
Kanpur

April, 2002

ACKNOWLEDGEMENT

Rabindra Nath Tagore had said, "My thoughts sit upon my words and dance", so I have too hope that a THANK YOU is going to express my gratitude towards all those who have helped in making this thesis a success.

With a profound sense of gratitude, I express my sincere thanks to my esteemed teacher and thesis supervisor Dr. S. P. Gupta for his invaluable guidance and encouragement throughout this work. I am indebted to him for providing me all the facilities and help in every possible way at IIT Kanpur.

I would also like to gratefully acknowledge Mr. R. P. Singh, Mr. M. N. Mungole and all the laboratory staff members of Dept. Of MME, IIT Kanpur, who directly or indirectly extended their co-operation for completion of this work. Thanks are due to all my friends who have made my stay at IIT Kanpur, a memorable and pleasant. Prominent amongst them are John, Siddharth, Sudhir, Vijay, Aditya, Shyam, Tapas, Sankar and Amit. Finally I must thank my labmates Indrani, Madhuri, Suresh for their kind support to successfully complete my work.

&

Last but not the least, I would like to thank my parents and family members, who have been a constant source of moral encouragement and inspiration to me.

Contents

List of Figures

List of Tables

Abstract

The morphology and growth kinetics of discontinuous precipitation of liquid and depleted solid phases from a supersaturated solid solution has been studied. The transformation was carried out in the two-phase (liquid + solid) field in the temperature range 723 to 777°C in two Cu-In alloys containing 8.9 and 9.5 at.pct. In using an optical microscope and electron probe microanalyser (EPMA). A lamellar structure consisting of alternate lamellae of α and liquid phases has been observed to grow from the grain boundaries of the supersaturated α. The nucleation of the liquid droplets occurred at the grain boundary and a thin layer of liquid formed between the droplets. The liquid film started migrating resulting in development of the lamellar structure. In both alloys, the growth rate increased with increasing temperature of transformation but the interlamellar spacing decreased with increasing transformation temperature. EPMA measurements indicated that the depleted matrix was richer in solute than the equilibrium solidus composition during the reaction. Electron probe microanalyser fitted with a super probe and metal standards has been used to determine the In concentration profiles across the liquid and solid lamella. These data, combined with the values of the reaction front velocity and the interlamellar spacing, have been used to analyze the growth kinetics using models after Cahn and Petermann and Hornbogen for cellular precipitation and mass balance using Fick's first law. From the diffusivity and activation energy values, it can be concluded that the growth of cellular structure occurs by solute transport through the thin layer of liquid formed between the transformed and untransformed regions of the matrix.

CHAPTER 1

INTRODUCTION

The kinetics of discontinuous precipitation during solid → solid transformation has been studied in a number of binary and ternary alloys (1 to 4). This includes Cu-In alloys (1). The transformation occurs by cellular precipitation reaction in which a supersaturated solid-solution (α_o) usually decomposes into a lamellar structure consisting of a new solute-rich precipitate phase (β) and a less-saturated initial phase (α) with the same crystal structure as the α_o according to the reaction:

$$\alpha_o \rightarrow \alpha + \beta.$$

The discontinuous precipitation of a liquid phase has been studied in Sb-Bi alloys in the past (5, 6). The planer growth front of the liquid/solid interface becomes unstable when a supersaturated solid solution is annealed in the two-phase, (liquid + solid (α)), region. The growth of the (solid + liquid) two-phase lamellar structure has been demonstrated for the Sb-Bi alloys by Kucharenko (6), who heated the supersaturated solid solution at a rate of up to $3X10^4$ Ks^{-1}. The Sb-Bi alloys were superheated by up to 70K above the solidus in the two-phase field. The migration distance of the discontinuously developed lamellar structure was reported to increase with the degree of superheating or by decreasing the rate of heating in the same alloy composition. A thin layer of liquid film appears to have formed at the migrating interface between the transformed and untransformed regions of the alloy. A similar transformation has been reported by Muschik et al (7) in Cu-In solid solutions during rapid heating above the solidus temperature.

The purpose of the present investigation is to study the kinetics of discontinuous precipitation of liquid and depleted α in a lamellar structure during transformation of the supersaturated α in two Cu-In alloys containing 8.9 and 9.5 at.pct. In. In the present study the technique of analytical electron microscopy was used to determine the solute

concentration profile across the liquid lamellae. The basic kinetic parameters of discontinuous precipitation of liquid were determined, following models after Cahn (8) and Petermann and Hornbogen (9) and mass balance.

1.1 SCOPE OF THE WORK

The thesis has been divided into four chapters.

In chapter 1, discontinuous precipitation is discussed. Three different models for the kinetics of discontinuous precipitation reaction are discussed in the same chapter.

The present investigation has been carried out on two alloys of copper containing 8.9 at.pct. In and 9.5 at.pct. In. The second chapter deals with the experimental procedures.

The kinetics of cellular reaction has been studied using theories of Cahn, Petermann and Hornbogen, and mass balance. The results obtained in both the cases are presented in the third chapter along with a detailed discussion.

In the fourth chapter the conclusions drawn from the results obtained are given.

1.2 DISCONTINUOUS PRECIPITATION

The formation of solute depleted α phase and a solute-rich precipitate phase in a lamellar morphology behind a grain boundary advancing into a supersaturated matrix has been termed as the discontinuous precipitation or cellular transformation. Investigations of growth kinetics of cellular precipitation in various systems have shown that the rate of migration of the cells is constant for a given temperature and alloy composition in the absence of other precipitation reactions. The rate of migration is controlled by the rate of diffusion of solute in the migrating grain boundary (8).

The initiation of this type of reactions has been studied in great detail. An early suggestion concerning why the reaction occurs in some alloys and not others was that a

minimum precipitate/matrix misfit parameter $\delta = \frac{a - a_o}{a_o}$ of 1% was necessary for the reaction to occur. Although this is based primarily on strain energy criterion, a number of alloy systems with a value of δ less than 1% decompose into lamellar products by discontinuous reaction. A similar concept was used by Bohm (10) for Cu-base alloys. Accordingly, the reaction would occur if the difference in diameters of solvent and solute atoms is more than 11%. Exceptions were reported even to this proposal as discontinuous precipitation reaction has been observed in Cu-Co alloys.

Meyrick (11) attempted to quantify the occurrence the reaction by cosidering a circular segment of a grain boundary pinned at points a distance '2r' apart, bulging forward a distance x, under the driving force for the reaction. It was postulated that the driving force has its origin in the change of grain boundary energy with the degree of solute segregation. If this change is high, the increase in grain boundary energy resulting from the grain boundary precipitation might be sufficient to induce the boundary to migrate in search of fresh solute. For discontinuous precipitation to occur, the following inequality should be satisfied.

$$-\frac{d\gamma}{dX_B} > \frac{2x\gamma}{({}^1X_B^\alpha - X_B^\alpha)r^2} \qquad (1.1)$$

where $-\frac{d\gamma}{dX_B}$ is the rate of decrease of the grain boundary energy with increase in concentration X_B at the boundary, ${}^1X_B^\alpha$ and X_B^α are the initial alloy and depleted matrix compositions, respectively. The inequality simply determines whether sufficient solute is incorporated into the boundary during the initial motion for the reaction to be energetically favourable. Thus, occurrence or not of the reaction will depend upon the segregation behaviour of the solute atoms. The measurement of the grain boundary energy is not accurate in most systems and this introduces an element of inaccuracy in the inequality of the equation 1.1. Moreover, there are many systems in which the composition dependent interfacial energy has been determined. Thus, it can be said that the formulation of simple models to predict discontinuous precipitation in a given alloy

system has not been very successful. The absence of discontinuous precipitation in a given alloy system on certain boundaries is a common variation. This indcates the sensitivity of reaction to individual grain boundaries on the one hand and to chemical driving force via supersaturation on the other.

With a large number of alloy systems showing cellular transformation, it has now been well established that solute rich precipitate always nucleates on the grain boundary and transformation occurs from the high mobility of the boundary. According to Smith (12), the cellular phase transformation occurs predominantly on those grain boundaries with a misorientation of more than 11°.

1.3 MORPHOLOGY OF CELLULAR REACTION

The initiation of discontinuous reaction is dependent on two factors, namely, the occurrence of heterogeneous grain boundary and the ability of the grain boundary to migrate. Thus the mechanisms can be classified into two categories:

1. Precipitation induced grain boundary migration,

2. Boundary migration due to chemical potential difference.

The Tu and Turnbull 'Pucker' mechanism (13) for discontinuous precipitation falls into the first category. The transformation of disc or plate shaped precipitate begins with nucleation on one side of a grain boundary having a high energy interface across the grain boundary and a low energy interface with the grain in which it is embedded. In order to bring both interfaces of the disc in a low energy configuration, a torque is created which makes the grain boundary migration resulting in local deflection of the grain boundary into a 'Puckered configuration' (13).

The interfacial energy imbalance between two broad faces of the precipitate can be eliminated by migration of grain boundary along the high energy interface, leaving the precipitate completely embedded in the grain but attached to the boundary at its tip. The initial driving force for the boundary migration is provided by the reduction in the interfacial energy of the precipitate. The boundary is now favourably oriented for the

nucleation of the second precipitate particle and the process of grain boundary migration repeats itself to build up a series of parallel lamellae which carry forward the boundary along as they migrate under the chemical driving force. This mechanism has been demonstrated in Pb-Sn alloys and is illustrated in Fig. 1.

No definite habit and orientation relationships have been found to exist in systems such as Fe-Zn (14), Cu-In (12) and the lamellae appears to have the ability to change direction and branch. In the mechanism proposed by, Fournelle and Clark (15) the thermally activated movement of the grain boundary like the grain boundary migration during normal grain growth is possible in the absence of precipitation and these are sufficient to stimulate the formation of cells if the boundary precipitation occurs concurrently.

A schematic diagram of the development of cellular structure from an initially unoccupied grain boundary is shown in Fig. 2, as suggested by Fournelle and Clark (15). Initially, the grain boundary will be subjected to the ordinary forces of boundary migration associated with a single phase alloy and will start to migrate accordingly, in this case to the right, Fig. 2a. However, after moving a short distance, allotriomorphs begin to form, pinning the boundary, Fig. 2b. the narrow region behind the migrating boundary is depleted of solute by boundary diffusion to the newly formed allotriomorph, and these pin the boundary. Further migration of the grain boundary is favoured because of compositional gradient across the boundary but possible if it bows between the precipitates (Fig. 2c), continuing to deplete the area behind it of solute. Fournelle and Clark (15) considered this to be critical step in the development of cell and suggested a criterion for reaction initiation based on free energy decrease.

1.4 GROWTH OF DISCONTINUOUS PRECIPITATE

A cell consists of a family of lamellae and the interlamellar spacing varies about the average value which remains constant at any aging temperature and increases with increasing temperature. The mechanism of growth of individual discontinuous cells is directly dependent on particular nucleation mechanisms that initiates the reaction.

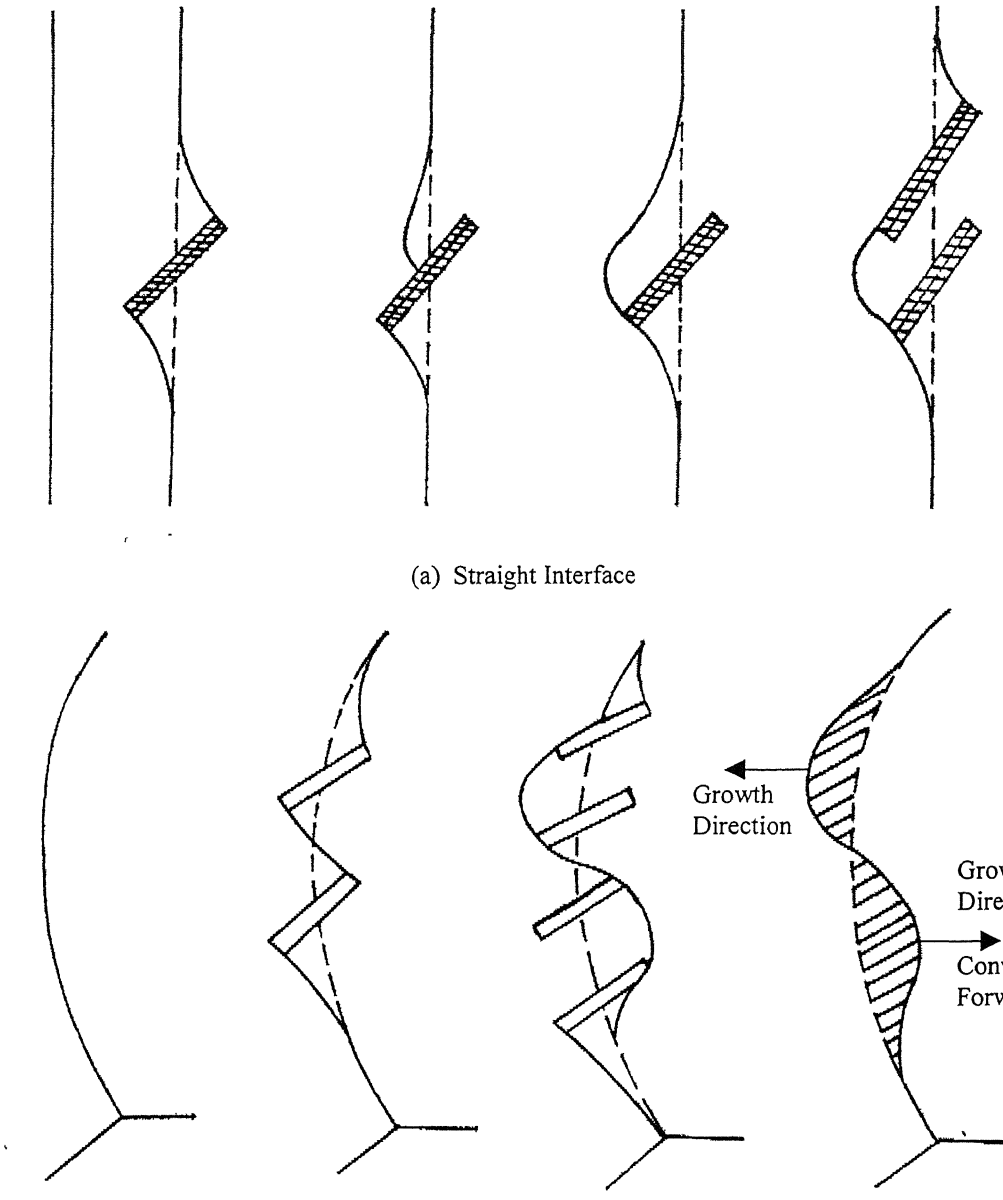

Fig. 1. Tu and Turnbull's Pucker Mechanism of cellular precipitation.

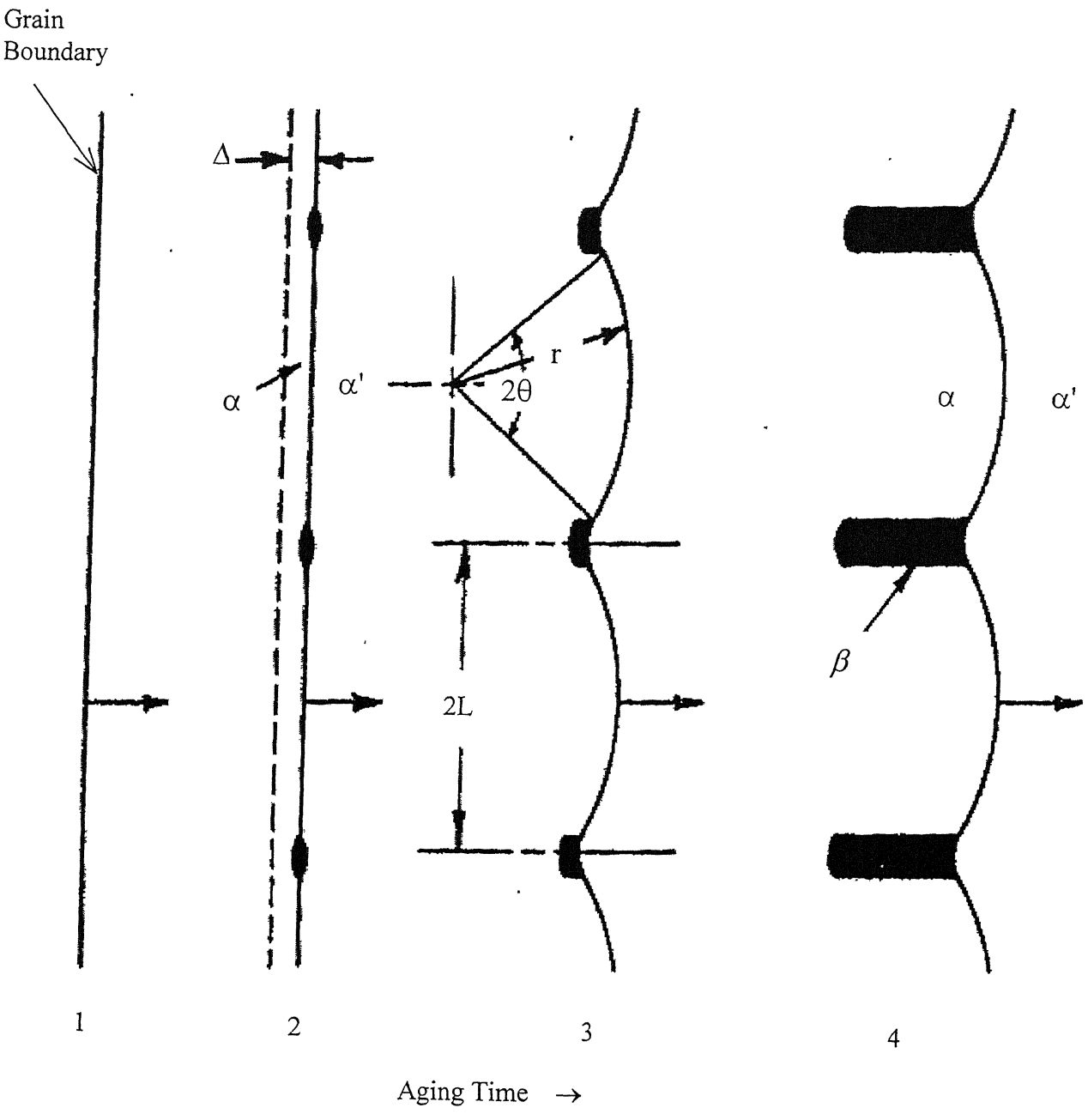

Fig. 2. Schematic diagram showing successive stages in nucleation of reaction on a migrating boundary, after Fournelle and Clark (15).

Growth may be in one or both directions. The mechanism of growth in one direction only is after Fournelle and Clark (15). The migration of grain boundary is presumed to be the dominant factor for cell growth. This operates in the temperature range where thermally activated migration of grain boundaries can occur. However, exceptions do exist to this proposal.

The development of cells in both the grains on either side of the grain boundary is a common observation. It is consequence of the 'Pucker' mechanism that cells nucleate in both the grains on adjacent segments of the grain boundary. The curvature of the grain boundary determines the cell growth direction and it is considered that a convex-forward growth is favoured.

The kinetics and morphology of the discontinuous precipitation reaction depends primarily on the nature of the diffusion path that transport and rearrange atoms. The cell boundary is the interface that separates the transformed from the untransformed regions (16). The solute atoms diffuse along moving grain boundaries to the precipitate, producing a solute depleted matrix behind the boundaries (17). Here the solute-rich precipitates act as sink for the solute atoms. The transformed regions of the cellular precipitation reaction consist of two phases in a lamellar morphology.

1.5 DISCONTINUOUS PRECIPITATION OF LIQUID PHASE

If a solid solution is heated to a temperature in the two-phase field above the solidus, it will be supersaturated. Its decomposition would involve precipitation of a solute-rich liquid and a depleted solid solution α (6). Liquid droplets nucleate on the grain boundaries and in a few seconds a continuous layer of liquid forms on them. Thereafter, the growth occurs by migration of the liquid/solid interfaces in a direction perpendicular to itself. Behind the migrating liquid/solid interfaces a lamellar structure characteristic of discontinuous precipitation develops, that is, colonies consisting of

liquid lamellae with cells of solid solution in between forms. The original supersaturated solid solution apparently goes over unselectively to the melt of the migrating interface; but the rate of decomposition depends on the rate of solute diffusion in the migrating layer of liquid, in accordance with the theories of Turnbull (18) and Cahn (8), and volume diffusion in the solid phase has no significance. The high rate of solute diffusion in the liquid phase makes the decomposition more rapid than is usually observed for the precipitation of a solid phase.

A solid solution of equilibrium composition is nucleated in the boundary layer of the melt and grows along it denuding the melt of the supersaturating component. The original supersaturated grains begin to dissolve in the denuded liquid surrounding a new bead of equilibrium solid solution of composition near the solidus. The layer of melt next to the bead of equilibrium solid solution have a composition near the equilibrium liquidus.

According to Kucherenko (6), the elastic stresses arising at the liquid/solid interface play a dominant role in forming the characteristic features of the products of cellular transformation. The binary system must have a considerable difference in the atomic diameters of the components. Under these conditions the uneven withdrawal of solute in the narrow zone of supersaturated matrix around the liquid gives rise to significant elastic stresses as a result of which the growth of the liquid in the solid phase is favourable in directions in which the matrix has the least elastic modulus. This accounts for the lamellar growth of the melt.

The kinetics of the discontinuous precipitation is controlled by diffusion along the migrating reaction front, and the maximum diffusion distance is equal to the half width of the α lamellae. Compositional changes resulting from these reactions can be measured using the technique of analytical electron microscopy (electron probe microanalyser). This study contributes a lot to the understanding of the mechanism and kinetics of the discontinuous precipitation reaction of a liquid phase.

1.6 DRIVING FORCE FOR DISCONTINUOUS PRECIPITATION

For the initiation of cellular phase transformation the following driving forces can be considered upon the mechanism of nucleation of the precipitate. Thus

$$\Delta G = \Delta G_{ppt} + \Delta G_{gb} + \Delta G_{\varepsilon} \qquad (1.1)$$

where ΔG_{ppt} arises from the chemical driving force due to compositional differences between supersaturated solid solution and depleted matrix.

The initial precipitate particles nucleate due to matrix supersaturation at the heat treatment temperature. Once nucleated, a small but finite amount of energy is released if both the interfaces of precipitate are embedded in the same grain that forms low energy interface with precipitate phase. The amount of energy released is used to deflect the grain boundary into an equilibrium position locally. In the mechanism of Nes and Bildal (19), the grain boundary moves under the chemical potential difference across the grain boundary, but it is pinned at the precipitate. Further migration is possible under chemical driving force for cellular precipitation.

In the mechanism proposed by Fournelle and Clark (15), the initial boundary migration occurs due to chemical potential difference across it to attain a low energy configuration. The migrating grain boundary deposits solute resulting in the nucleation of precipitate. The boundary continues migration under the chemical driving force for the cellular phase transformation. The solute diffusion through grain boundary continues as it sweeps through the supersaturated matrix thus supplying more solute to the growing precipitate phase. A part of chemical driving force for initiation may be used in the form of strain energy, ΔG_{ε}, if the atomic diameter of solute and solvent are significantly different. However in alloy systems with comparable atomic diameters, strain energy does not play a major role.

1.7 MODELS FOR KINETICS OF DISCONTINUOUS PRECIPITATION

1.7.1 Cahn's Treatment of discontinuous precipitation

It has been realized by Cahn (8) that the α lamellae in equilibrium with β phase is not of equilibrium composition. Due to incomplete segregation of solute only a fraction of total free energy available will be used to drive the reaction. A part of the available free energy ($p\Delta G^{\circ}+\frac{2\gamma V_m}{\lambda}$) will be used as chemical free energy out of which $\frac{2\gamma V_m}{\lambda}$ will be associated with the newly formed interface. It has been pointed out by Cahn (8) that if the rate of migration of cell boundary is finite, then solute precipitation will be incomplete. This result in higher average concentration of solute in the depleted α matrix after completion of cellular reaction. It is assumed that reaction proceeds as far as diffusion permits and that the interface is flat and no diffusion occurs except at the boundary. Under steady state conditions,

$$\frac{dX_B^{\alpha}}{dt}=\frac{D_b}{V_m}.\frac{d^2X_B^{b}}{dx^2}+\frac{v}{V_m\delta}\left({}^{1}X_B^{\alpha}-X_B^{\alpha}\right)=0 \qquad (1.2)$$

where v is the growth velocity, ${}^{1}X_B^{\alpha}$, X_B^{α} are the original alloy composition and composition of solute in the depleted matrix, respectively, x is the distance along the boundary measured perpendicular to the lamellae and V_m is the molar volume.

Assuming X_B^{α} to be proportional to X_B^{b} with a proportionality constant k (defined as segregation ratio), which is $X_B^{b}/X_B^{\alpha}=k=$ constant, equation (1.2) can be solved. Equilibrium exists at the α/β interface and that β lamellae are thin as compared to λ (interlamellar spacing), so that the boundary conditions are

$$X_B^{\alpha}={}^{e}X_B^{\alpha} \quad \text{at} \quad x=\pm\lambda/2$$

and the above equation can be solved to yield

$$\alpha = \frac{v\lambda^2}{kD_b\delta}, \qquad (1.3)$$

where α can be determined from the fraction of the solute precipitated. It is related to the compositions from the relation

$$\frac{{}^{1}X_B^{\alpha} - X_B^{\alpha}}{{}^{1}X_B^{\alpha} - {}^{e}X_B^{\alpha}} = \frac{2}{\sqrt{\alpha}} \tanh\left(\frac{\sqrt{\alpha}}{2}\right), \qquad (1.4)$$

where ${}^{e}X_B^{\alpha}$ is the equilibrium solvus composition.

1.7.2 Petermann and Hornbogen's treatment

According to Petermann and Hornbogen (9), growth velocity is given by

$$v = -M.\,\Delta G \qquad (1.6)$$

where M is the grain boundary mobility and ΔG is the driving force for growth of the cells.

The mobility is a function of temperature and is determined by atomic jump frequency τ^{-1} and grain boundary thickness δ. For the phase to grow and therefore for the continued migration of the grain boundary, solute atom acquired by the grain boundary must diffuse a distance $\lambda/2$ to the β lamellae. The time for atoms to move a distance $\lambda/2$ is

$$\frac{\lambda^2}{4} = 2D_b\tau$$

therefore,

$$\tau = \frac{\lambda^2}{8D_b}$$

which gives

$$D_b\delta = -\frac{v\lambda^2 RT}{8\Delta G} \tag{1.6}$$

where T is the isothermal transformation temperature in K and ΔG is the driving force which can be calculated from the compositions and the activity data for solute and solvent in solid solutions. The ΔG value can be estimated from the equation

$$\Delta G = \Delta G^C + \Delta G^\gamma$$

where ΔG^C and ΔG^γ are the chemical free energy and surface free energy, respectively. These are given by the equations:

$$\Delta G^C = RT\left[{}^1X_B^\alpha \ln\frac{a_B^\alpha}{{}^1a_B^\alpha} + {}^1X_A^\alpha \ln\frac{a_A^\alpha}{{}^1a_A^\alpha}\right] \tag{1.7}$$

$$\Delta G^\gamma = \frac{2\gamma V_m}{\lambda} \tag{1.8}$$

where a_B^α, ${}^1a_B^\alpha$ are the activities of solute in the depleted matrix and original alloy compositions, respectively and a_A^α, ${}^1a_A^\alpha$ are the activities of solvent in the depleted matrix and original alloy compositions, respectively in the alloy. γ is the specific surface energy of the α/β interface.

1.7.3 Mass balance model

Let us consider the precipitation of β-phase from a supersaturated solid solution, forming a lamellar morphology. Using Turnbull's model of cellular precipitation (18), based on diffusion of solute through the grain boundary, the flux of solute rejected during growth of the α lamellae equals the flux of solute through the grain boundary at the migrating interface. The diffusion equation can be written as

$$\frac{vb}{V_m}({}^1X_B^\alpha - X_B^\alpha)\lambda^\alpha = -\frac{A^b D_b}{V_m}\frac{\partial X_B^b}{\partial x} \tag{1.9}$$

which gives

$$D_b\delta = -\frac{v\lambda^2 RT}{8\Delta G} \tag{1.6}$$

where T is the isothermal transformation temperature in K and ΔG is the driving force which can be calculated from the compositions and the activity data for solute and solvent in solid solutions. The ΔG value can be estimated from the equation

$$\Delta G = \Delta G^C + \Delta G^\gamma$$

where ΔG^C and ΔG^γ are the chemical free energy and surface free energy, respectively. These are given by the equations:

$$\Delta G^C = RT\left[{}^1X_B^\alpha \ln\frac{a_B^\alpha}{{}^1a_B^\alpha} + {}^1X_A^\alpha \ln\frac{a_A^\alpha}{{}^1a_A^\alpha}\right] \tag{1.7}$$

$$\Delta G^\gamma = \frac{2\gamma V_m}{\lambda} \tag{1.8}$$

where a_B^α, ${}^1a_B^\alpha$ are the activities of solute in the depleted matrix and original alloy compositions, respectively and a_A^α, ${}^1a_A^\alpha$ are the activities of solvent in the depleted matrix and original alloy compositions, respectively in the alloy. γ is the specific surface energy of the α/β interface.

1.7.3 Mass balance model

Let us consider the precipitation of β-phase from a supersaturated solid solution, forming a lamellar morphology. Using Turnbull's model of cellular precipitation (18), based on diffusion of solute through the grain boundary, the flux of solute rejected during growth of the α lamellae equals the flux of solute through the grain boundary at the migrating interface. The diffusion equation can be written as

$$\frac{vb}{V_m}({}^1X_B^\alpha - X_B^\alpha)\lambda^\alpha = -\frac{A^b D_b}{V_m}\frac{\partial X_B^b}{\partial x} \tag{1.9}$$

where A^b is the area through which diffusion takes place and it is equals to $2b\delta$, where δ is the grain boundary thickness and b is the distance parameter perpendicular to the growth direction and α/β interface. D_b is the diffusion coefficient of solute in the boundary, V_m is the molar volume, and $\frac{\partial X_B^b}{\partial x}$ is the concentration gradient along the migrating boundary.

$$\frac{v}{V_m}({}^1X_B^\alpha - X_B^\alpha)\lambda^\alpha = -\frac{2D_b\delta}{V_m}\frac{\partial X_B^b}{\partial x} \qquad (1.10)$$

Since segregation ratio is $k = \frac{X_B^b}{X_B^\alpha}$, $\partial X_B^b = k\,\partial X_B^\alpha$

Equation (1.10) becomes

$$\frac{v}{V_m}({}^1X_B^\alpha - X_B^\alpha)\lambda^\alpha = +\frac{2kD_b\delta}{V_m}\frac{\Delta X_B^\alpha}{\Delta x} \qquad (1.11)$$

Δx is the effective diffusion distance and has been estimated as $\frac{\lambda^\alpha}{2}$. Also λ^α, width of α lamellae, is related by lever's principle as

$$\lambda^\alpha = \frac{\left(X_B^\beta - {}^1X_B^\alpha\right)}{\left(X_B^\beta - X_B^\alpha\right)}.\lambda = f^\alpha.\lambda \qquad (1.12)$$

where f^α is the fraction of the α phase in the two phase structure. Equation (1.11) can be written as

$$v(f^\alpha)^2\lambda^2({}^1X_B^\alpha - X_B^\alpha) = 4kD_b\delta.\Delta X_B^\alpha \qquad (1.13)$$

which gives $$kD_b\delta = \frac{v\lambda^2(f^\alpha)^2.({}^1X_B^\alpha - X_B^\alpha)}{4({}^1X_B^\alpha - {}^eX_B^\alpha)} \qquad (1.14)$$

1.8 Copper-Indium system

The phase diagram of Cu-In system is given in Fig. 1 (20). The phase diagram pertinent to the regions of temperature and concentration in which precipitation has been investigated is given in Fig. 2 (21), where Cu-8.9 at.pct. In and Cu-9.5 at.pct. In alloy compositions are shown by line a and b respectively. The liquid phase is precipitated out in the temperature range in which precipitation kinetics were studied.

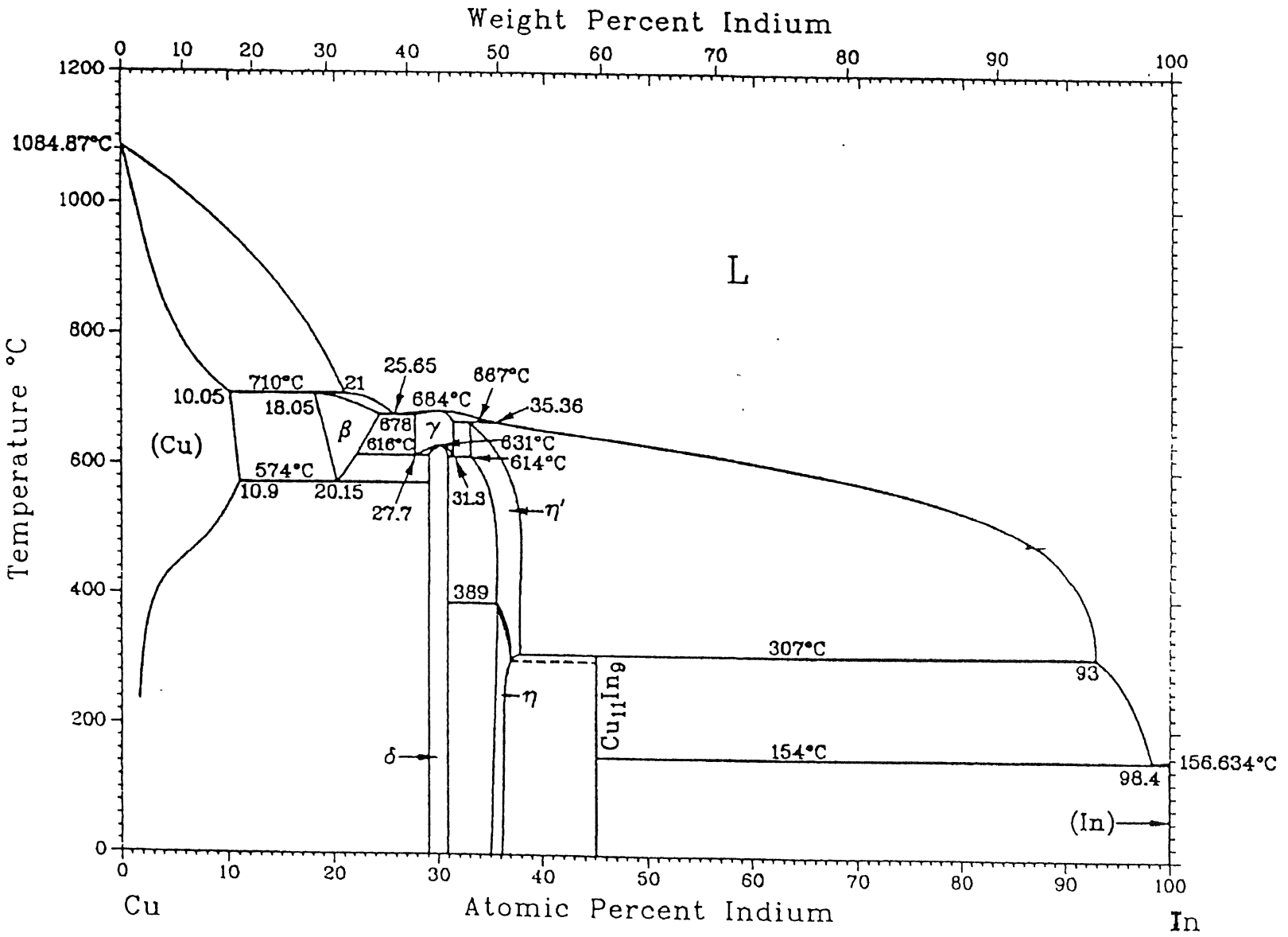

Fig. 3. The Cu-In binary phase diagram.

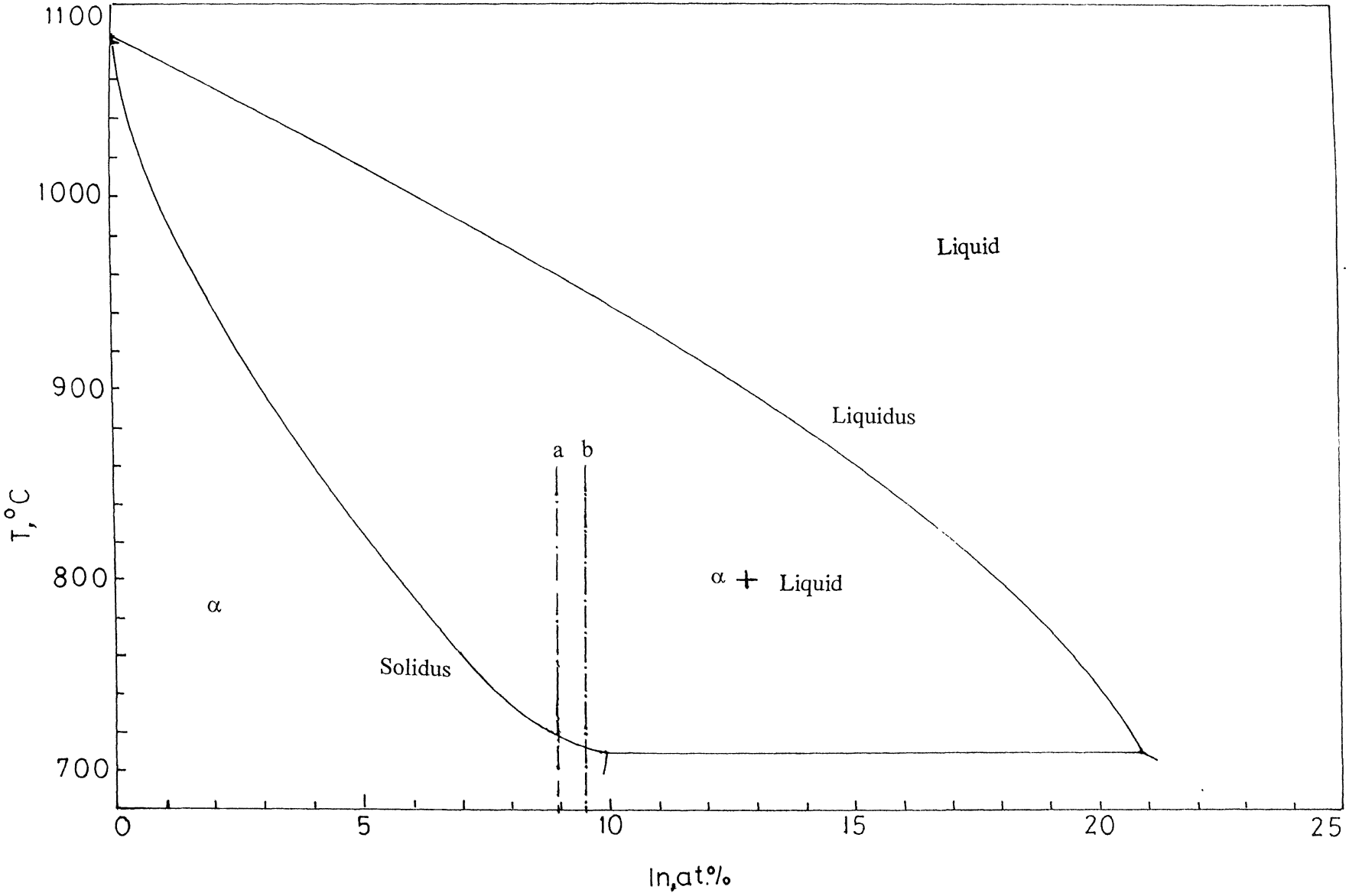

Fig. 4. Part of the Cu-In phase diagram in which precipitation reaction has been investigated.

CHAPTER 2

EXPERIMENTAL PROCEDURE

The alloys for this investigation were prepared by melting together Cu and In both of 99.99% purity in sealed silica tubes under vacuum. Two alloy compositions Cu-8.9 at.pct. In (15wt.pct.) and Cu-9.5 at.pct. In (16wt.pct.) were prepared by keeping the silica tubes at 1100°C for 12 hours. The liquid was shaken a few times during mixing of the two liquid metals. The liquid was solidified and silica tubes were broken while at the ambient temperature. Subsequently, the alloy rods were homogenized at 700°C for 7 days to remove microsegregation and subsequently quenched. The 8mm diameter alloy rods were cold rolled to a thickness of 1mm. Small sheet samples measuring approximately 6mm x 8mm were cut from the rolled sheet. These were subsequently ground on emery paper to remove surface contamination. A number of sheet samples were annealed at 700°C for 24 hours in sealed silica tubes under vacuum and quenched in a mixture of ice and water. A polycrystalline structure with a grain size of the order of 250μm has developed.

In order to carry out the transformation, the specimens were transferred to a salt bath maintained at the desired temperature. The specimens were wrapped in Cu-foils in order to prevent the salt from getting in direct contact with the liquid that formed during transformation in the (liquid + solid) two-phase field. Each heat-treated specimen was quenched in ice and water mixture at about 4°C. A number of specimens were heat treated to take care of the time and temperature dependence of the transformation. The specimens were mounted and prepared for metallographic examination using standard metallographic techniques. Each specimen was etched with a potassium dichromate etchant.

The average velocities of the migrating front for the discontinuous precipitation were obtained from light microscopy measurements of the widths of migration distance as a function of annealing time. In order to accomplish this, about 40-50 measurements of the growth distance from the original position of the grain boundary to the leading

edge of the migrating boundary were taken. Only those colonies, in which the lamellar structure was regular, were analyzed. The slope of the plot of this cell width versus annealing time was taken as the migration rate.

Interlamellar spacing measurements were made using an optical microscope fitted with a reticule. Fifty randomly chosen spacing were measured and averaged.

The composition profile across the liquid and solid lamellae was obtained using electron probe microanalyser (JEOL model 8600 MX) fitted with a super probe and metal standards.

CHAPTER 3

EXPERIMENTAL RESULTS AND DISCUSSION

3.1 Morphology

The microstructure observed through the optical microscope revealed that the transformation of the supersaturated solid solution (α) into solute rich liquid and depleted α occurred at all temperatures in the range 723 to 757°C and 737°C to 777°C in Cu-9.5 at.pct. In and Cu-8.9 at.pct. In alloys, respectively. The product phases formed into a lamellar structure consisting of alternate lamella of α and liquid phases. The nucleation of the liquid in the form of small droplets can be clearly observed in the photomicrograph of Fig.5 derived from a specimen heat treated for 10 s at 723°C. The nucleation of the liquid has occurred at the grain boundaries of the parent phase and there appears to be an abundance of the nuclei to the extent that some of them have merged together and have formed a continuous layer of the liquid.

The growth of the liquid lamellae occurs by the formation of a liquid film between the parent and depleted α phases. The liquid film starts to migrate with increasing time of transformation in the (α+L) phase fields as is apparent from the photomicrograph of Fig. 6. The formation of a thin liquid layer between the parent and depleted α was also demonstrated by Kucharenko (6) in the Sb-Bi system. The transformation is very similar in a way to what has been observed during cellular or discontinuous precipitation in the Cu-In system (1) as well as in other binary and ternary alloy systems. The only difference between the two is that whereas the solute transport occurs through the grain boundaries during growth of the cellular precipitate, it occurs through a thin layer of liquid during solid to liquid transformation.

The lamellar structure develops after some growth of the cell. The liquid film migrates into one of the grains from its initial position near the grain boundary as is apparent from the photomicrograph of Fig. 7. The lamellar structure also developed on

the both sides of the grain boundary in another region of the same specimen, Fig. 8. The formation and growth of the cells either on one side of the grain boundary or on the other sides of it has also been observed during cellular precipitation in a number of alloy systems and it is a common occurrence. The phenomenon is generally related to the grain boundary curvature. It has generally been observed that whereas the cells grow only on one side of the planar grain boundary they grow on both sides of curved boundaries.

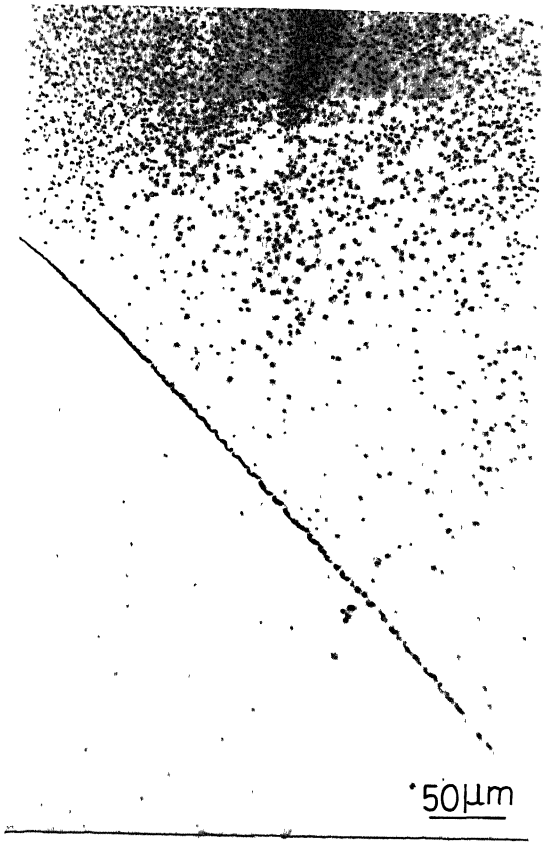

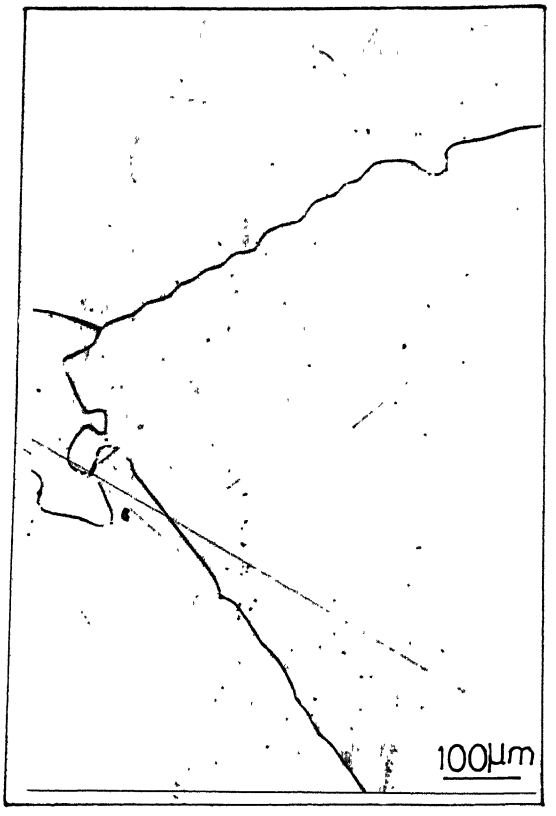

Fig. 5 **Fig. 6**

Fig. 5. Optical photomicrograph showing nucleation of liquid droplets at the grain boundaries. A thin layer of liquid has formed between the droplets and has just started migrating, 10s at 723°C, Cu-9.5 at.pct. In alloy.

Fig. 6. The migration of the liquid film can be clearly observed between liquid droplets on few grain boundaries of α, 10s at 723°C, Cu-9.5 at.pct. In alloy.

An interesting structure of the interface doubling up is shown in Fig. 9. The liquid film has started moving forward with the liquid lamellae trailing behind. In the region of migrating interface where the distance between liquid lamellae are large, the solute starts building up in the middle and forms a recess. The interface finally doubles up leaving a loop of liquid film. One such loop can be clearly seen in the photomicrograph of Fig. 9 and another is in the process of formation nearby. The formation of recess and doubling up of the interface results from high rate of migration when the time for solute transport is insufficient as suggested by Sundquist (22) during austenite to pearlite transformation.

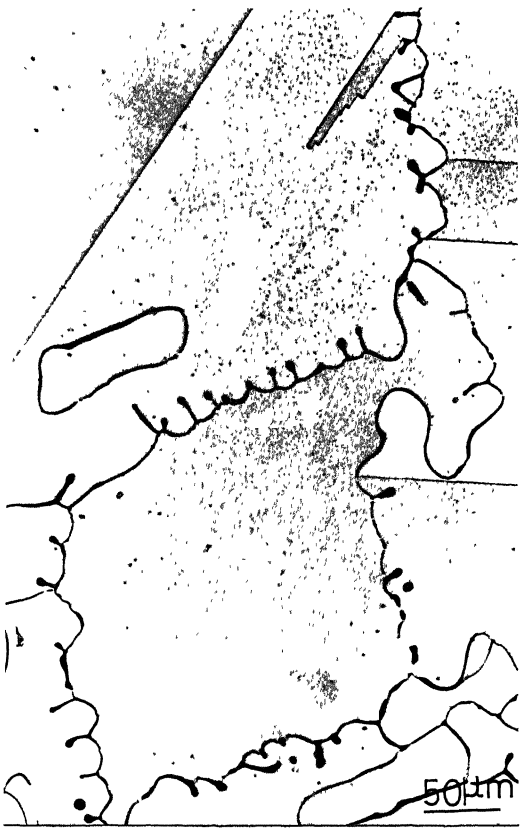

Fig. 7 **Fig. 8**

Fig. 7. Optical photomicrograph showing development of the lamellar structure, 21s at 723°C, Cu-9.5 at.pct. In alloy.

Fig. 8. Optical photomicrograph showing lamellar structure on both sides of the prior grain boundaries, 25s at 723°C, Cu-9.5 at.pct. In alloy.

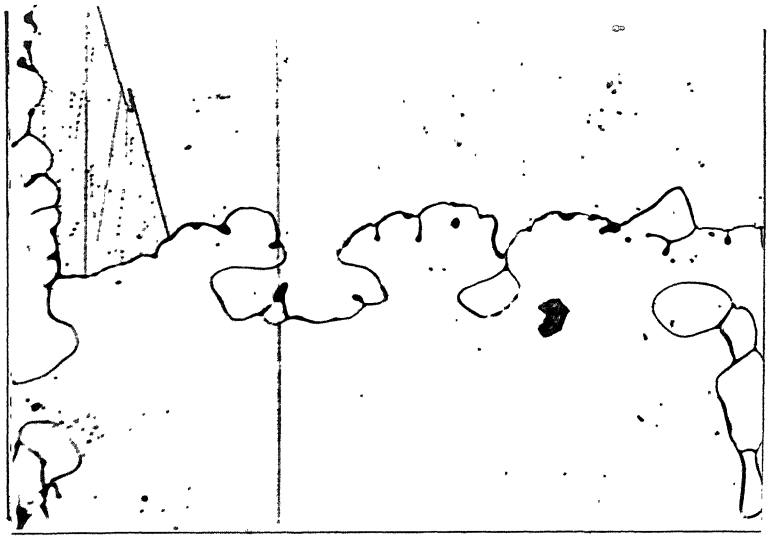

Fig. 9. A cylindrical region of the α phase has formed in the recess behind a migrating front where the lamellae are widely spaced. A similar cylindrical region in the neighborhood is in the process of formation, 16s at 723°C.

A well developed lamellar structure forms in the specimens isothermally transformed for longer distance as can be observed in Figs. 10a and 10b. From the microstructure it appears that although the liquid film starts migrating with few liquid lamellae tracking behind, the rapid migration leads to nucleation of new lamellae in the recess as well as on the curved migration front. The nucleation in the recess is due to high migration rate of the interface and on the curved interface it is to reduce the ever increasing migration distance. The observation is consistent with the microstructures observed during cellular precipitation reaction.

The higher superheating (higher ΔT) or longer time at lower transformation temperature (low ΔT), the liquid droplets were also observed in the central region of the grain, Fig. 11. Some of the droplets coalesced to form a cylinder of the liquid phase. The cellular structure was observed, however, near the original grain boundary, Fig. 11. The observation is consistent with the results presented by Kucherenko (6) for the Sb-Bi alloy.

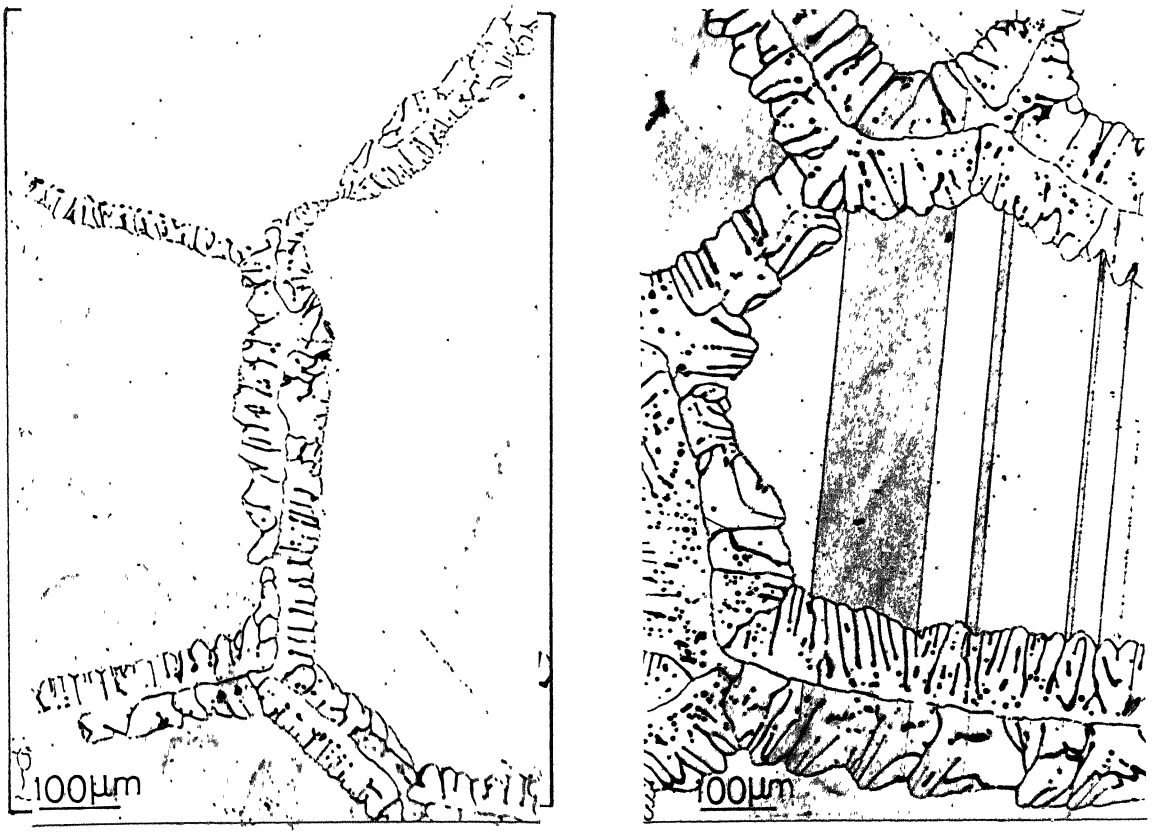

(a) (b)

Fig. 10. Optical photomicrograph showing well developed lamellar structure, (a) 30s at 723°C and (b) 35s at 723°C, Cu-9.5 at.pct. In alloy.

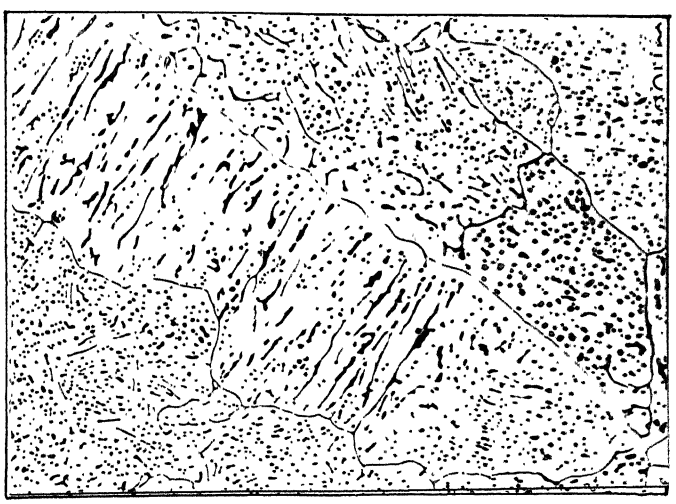

Fig. 11. The microstructure reveals the general precipitation in the central region of the grain and the lamellar structure near the original grain boundary of the α phase, 30s, 742°C, Cu-9.5 at.pct. In alloy.

3.2 Growth Rate

The growth rate of the cell was determined by measuring the migration distance from the original position of the grain boundary to the leading edge of the cell. Forty measurements were made randomly from each specimen and the data averaged. The growth distance was plotted against the time of transformation at each temperature, Fig. 12. There appears to be a linear relationship between the growth distance and time of transformation as has been observed during cellular phase transformation. The rate of growth was determined from the slope of the straight line which best fits the data points. The rate of growth is plotted in Fig. 13 as a function of temperature (for the two alloy compositions studied).

The growth rate increases with increasing temperature of transformation. Moreover, the rate of migration of the cell boundaries is higher for the Cu-9.5 at.pct. In alloy at all temperatures when compared with the data for the Cu-8.9 at.pct. In alloy. There is more than an order of magnitude difference in the rate of growth of cells in a temperature interval of about 40K. For the Cu-8.9 at.pct. In alloy, the rate of growth of cells lies in the range $1.36X10^{-6}$ ms^{-1} to $2.5X10^{-5}$ ms^{-1}, which is two to three order of magnitude higher than the maximum growth rate of $1.1X10^{-8}$ ms^{-1} obtained at 392°C during cellular precipitation to ($\alpha+\delta$) in the same alloy composition (1). The transformation was very rapid at the highest temperature of 777°C used in this investigation, which is approximately 60K above the solidus temperature for the Cu-8.9 at.pct. In alloy. The rate of growth of cells in the Cu-9.5 at.pct. In alloy are two to three times faster than those in the Cu-8.9 at.pct. In alloy.

3.3 Interlamellar Spacing

The interlamellar spacing data was measured at each temperature from specimens with well developed cell and about forty measurements were made and the data averaged. The interlamellar spacing, λ, data for the two alloy compositions are shown in Fig. 14. There was some variation in the interlamellar spacing from one cell to the other.

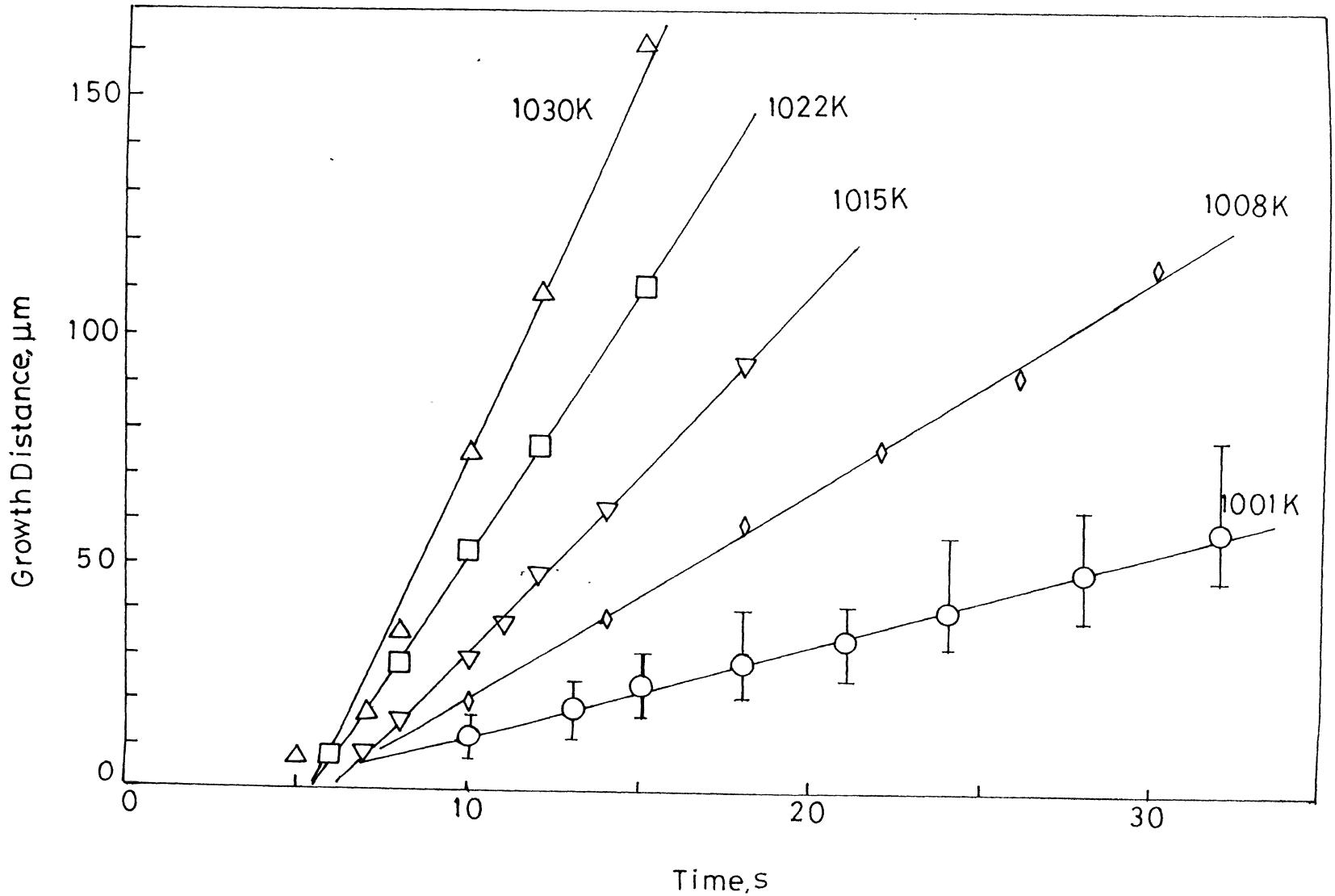

Fig. 12 (a) Growth distance vs time plot, for Cu-9.5 at.pct. In alloy.

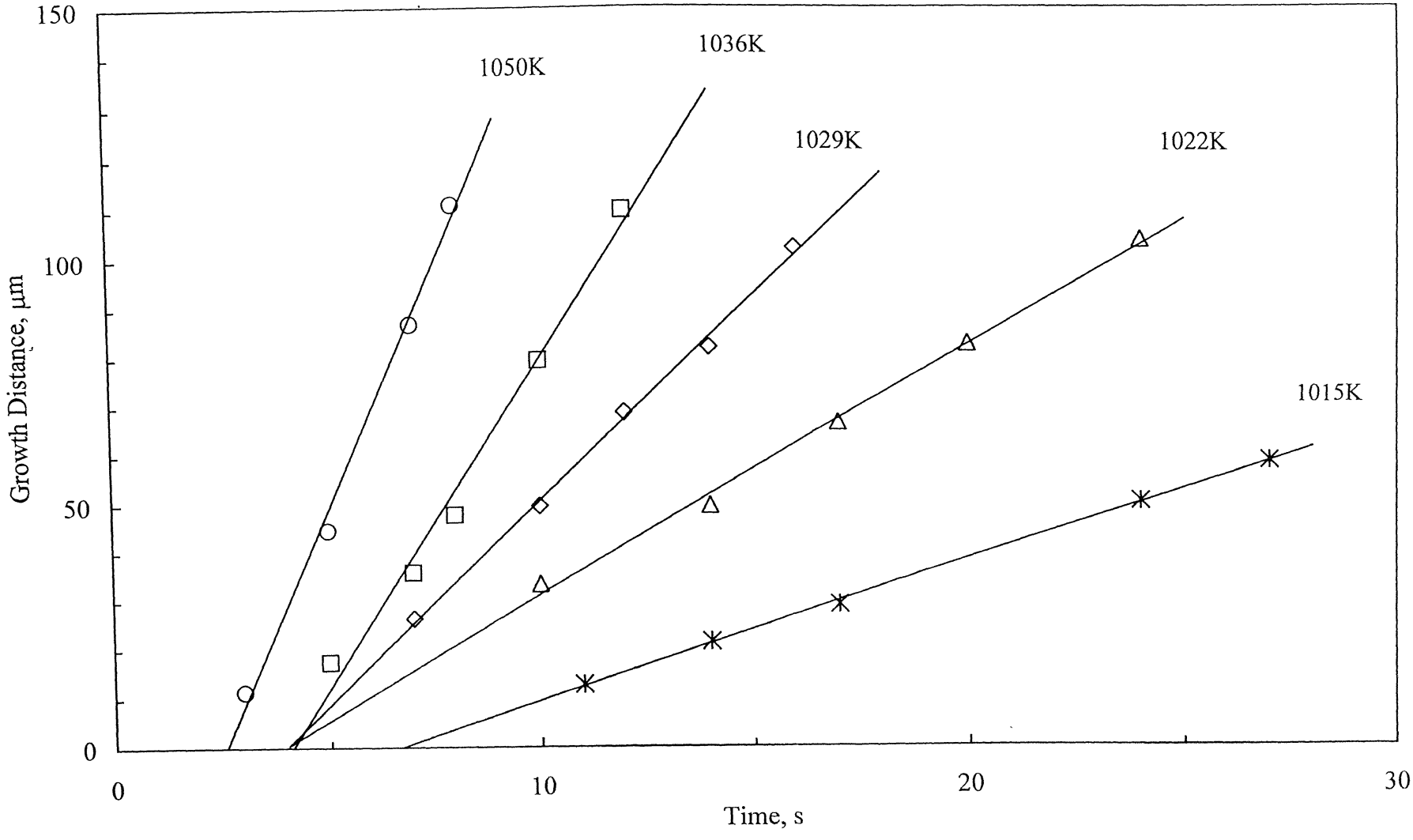

Fig. 12 (b). Growth distance vs time plot, for Cu-8.9 at.pct. In alloy.

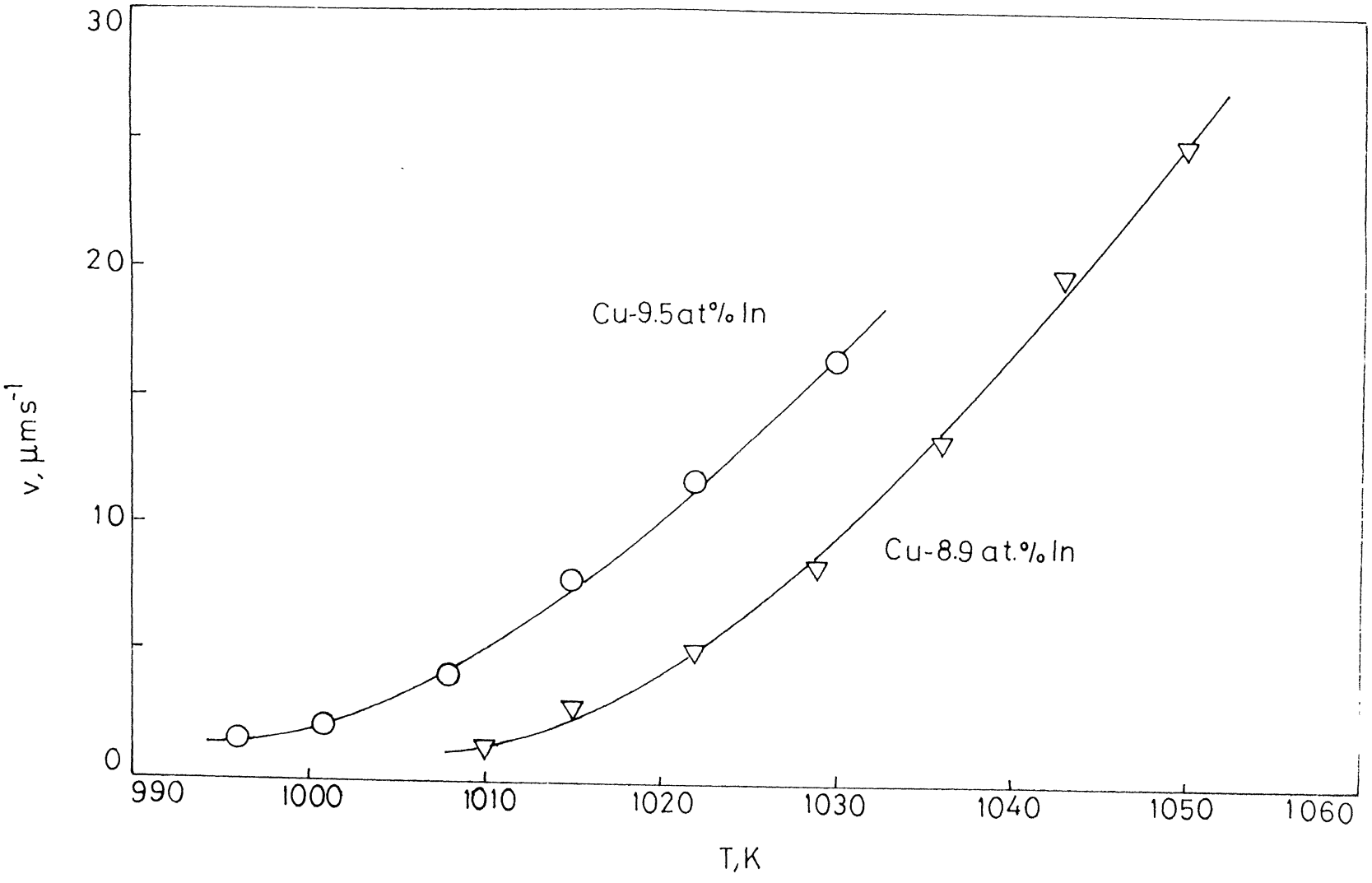

Fig. 13.Growth rate (v) vs transformation temperature.

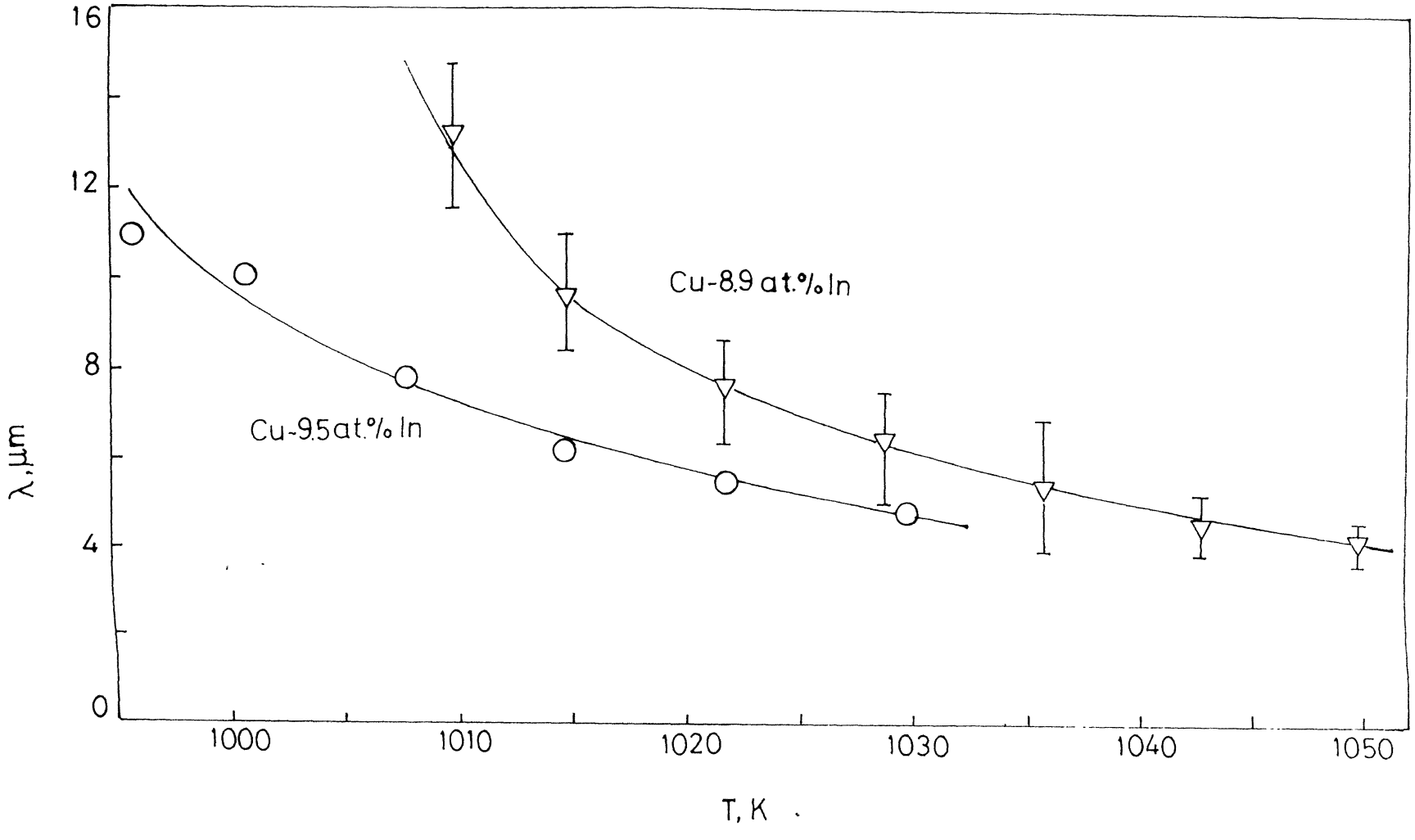

Fig. 14. Interlamellar spacing vs transformation temperature.

This is expected because of variation in the growth rate of cells originating from different grain boundaries of the supersaturated α and is dependent on the initial structure of the grain boundaries. The interlamellar spacing decreases with increasing transformation temperature for both alloy compositions. The interlamellar spacing of cells in the Cu-8.9 at.pct. In alloy is higher than those of the Cu-9.5 at.pct. In alloy at all temperatures by a factor of approximately two. This is expected from results of the growth rate in the two alloy compositions. The interlamellar spacing lies in the range $5X10^{-6}$m to $1.3X10^{-5}$ m. In comparison the maximum interlamellar spacing of cells in the Cu-8.9 at.pct. In alloy during cellular precipitation is reported (1) to be 1.1×10^{-6}m at 454°C which is an order of magnitude lower than the maximum interlamellar spacing observed in this investigation during growth of cells consisting of alternate lamellae of liquid and solute depleted α phases.

The thickness of the migrating liquid film has been measured in an under etched specimen to lie in the range 0.2 to 0.3 micrometers.

3.4 Composition of the liquid and depleted matrix

The composition of the depleted matrix was determined by carrying out concentration-distance profile across the lamellar structure covering both liquid and α phases using electron probe microanalyser (EPMA). The solute profiles across the *liquid* lamellae play an important role in the local characterization of the discontinuous precipitation reaction. In the present case only those lamellae which were exhibiting parallel growth were chosen for the EPMA analysis, using steps of 1 μm. A few concentration-distance profiles are presented in Fig. 15 a, b and c. The composition of the liquid lamellae was observed to be close to the liquidus composition at each temperature. The profiles clearly reflect the excess indium content within the *liquid* lamellae. They are symmetrical with respect to the middle of the *liquid* lamellae. However, due to small thickness of the liquid lamellae (λ^L) the exact composition of the liquid could not be ascertained. The width of the depleted matrix was observed to be higher and it was possible to get composition with small variation about the average

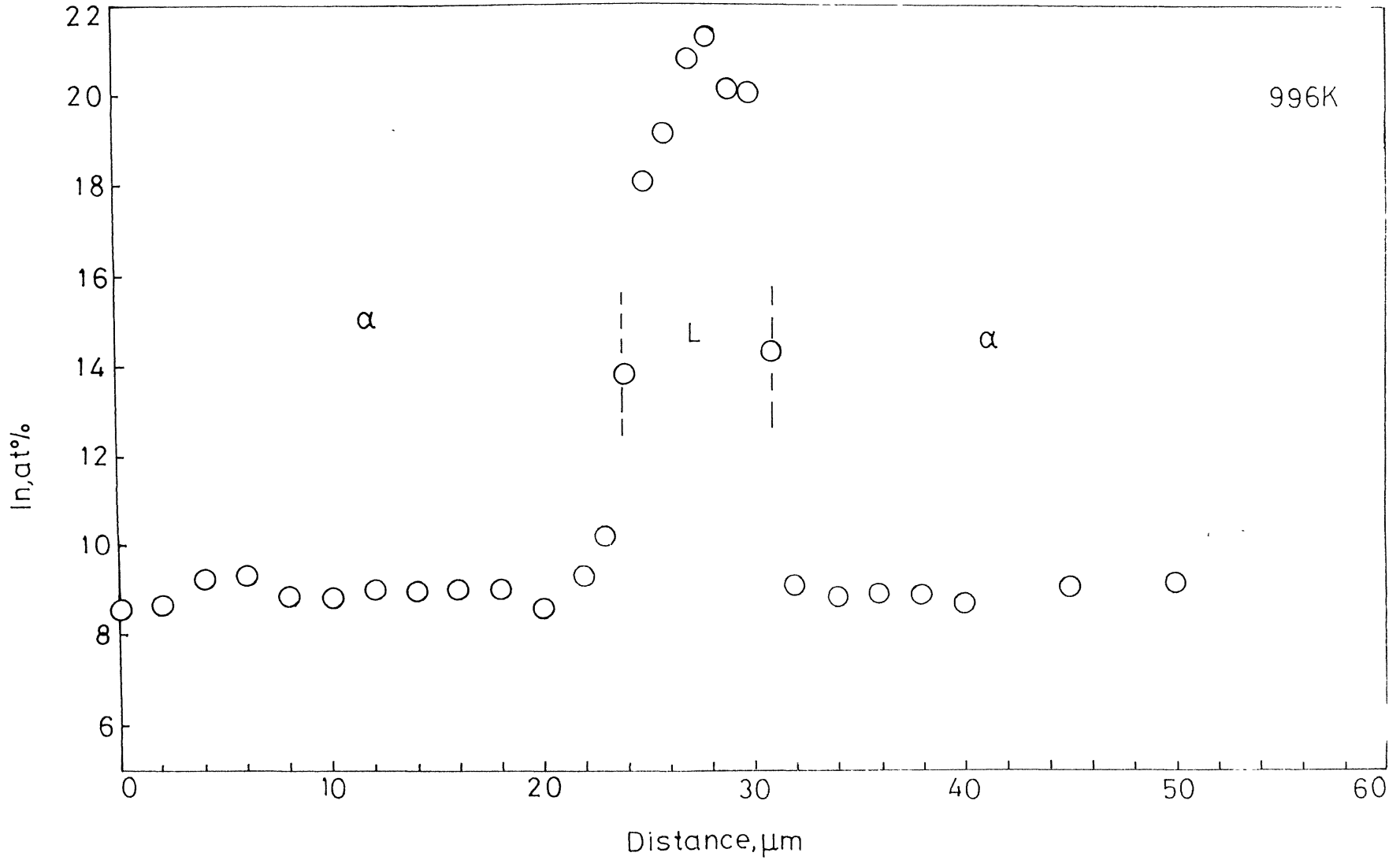

Fig. 15 a. Composition profile of In across the lamellar structure, 723°C, Cu-9.5 at.pct. In alloy.

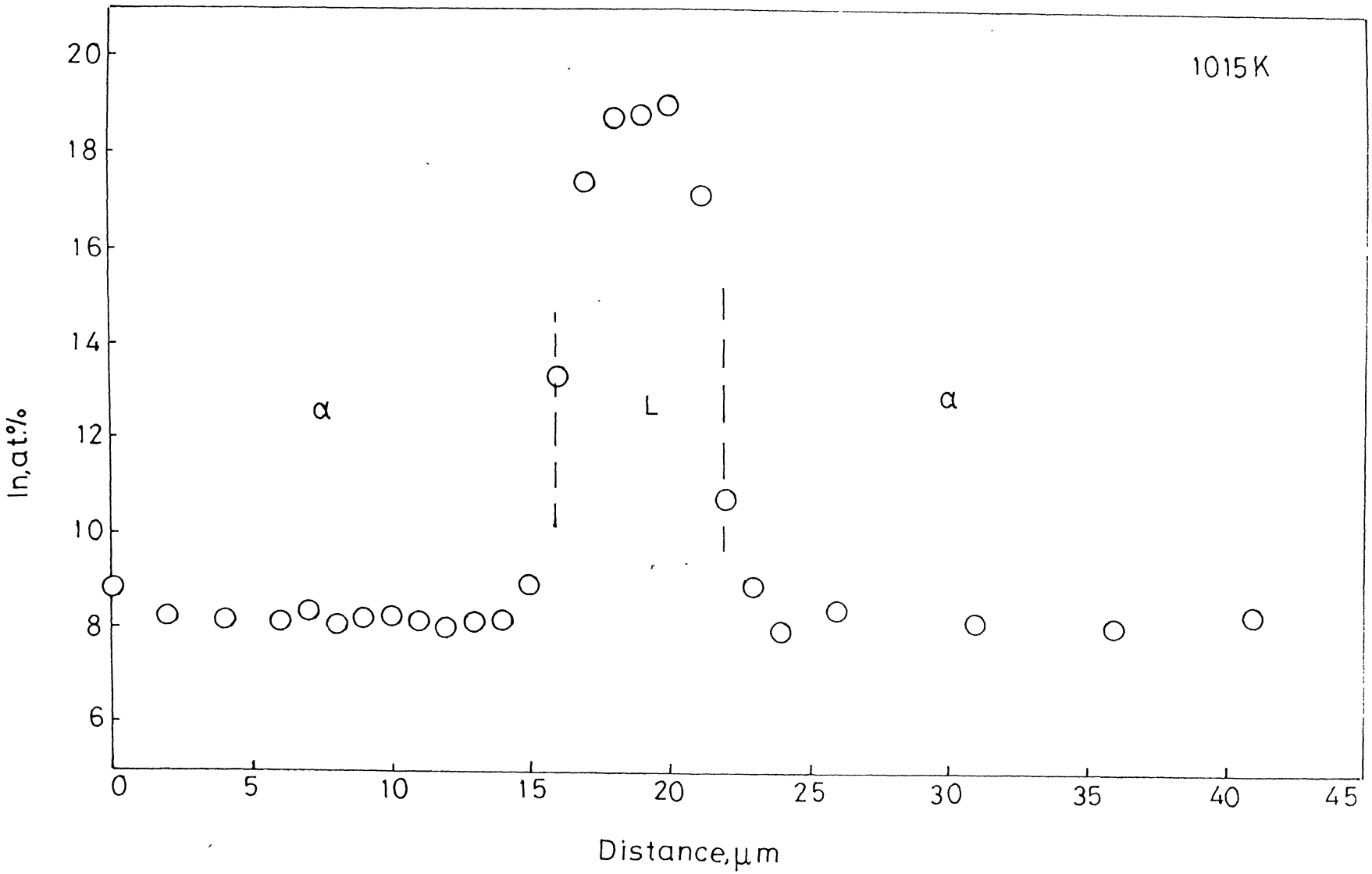

Fig. 15 b. Composition profile of In across the lamellar structure, 735°C, Cu-8.9 at.pct. In alloy.

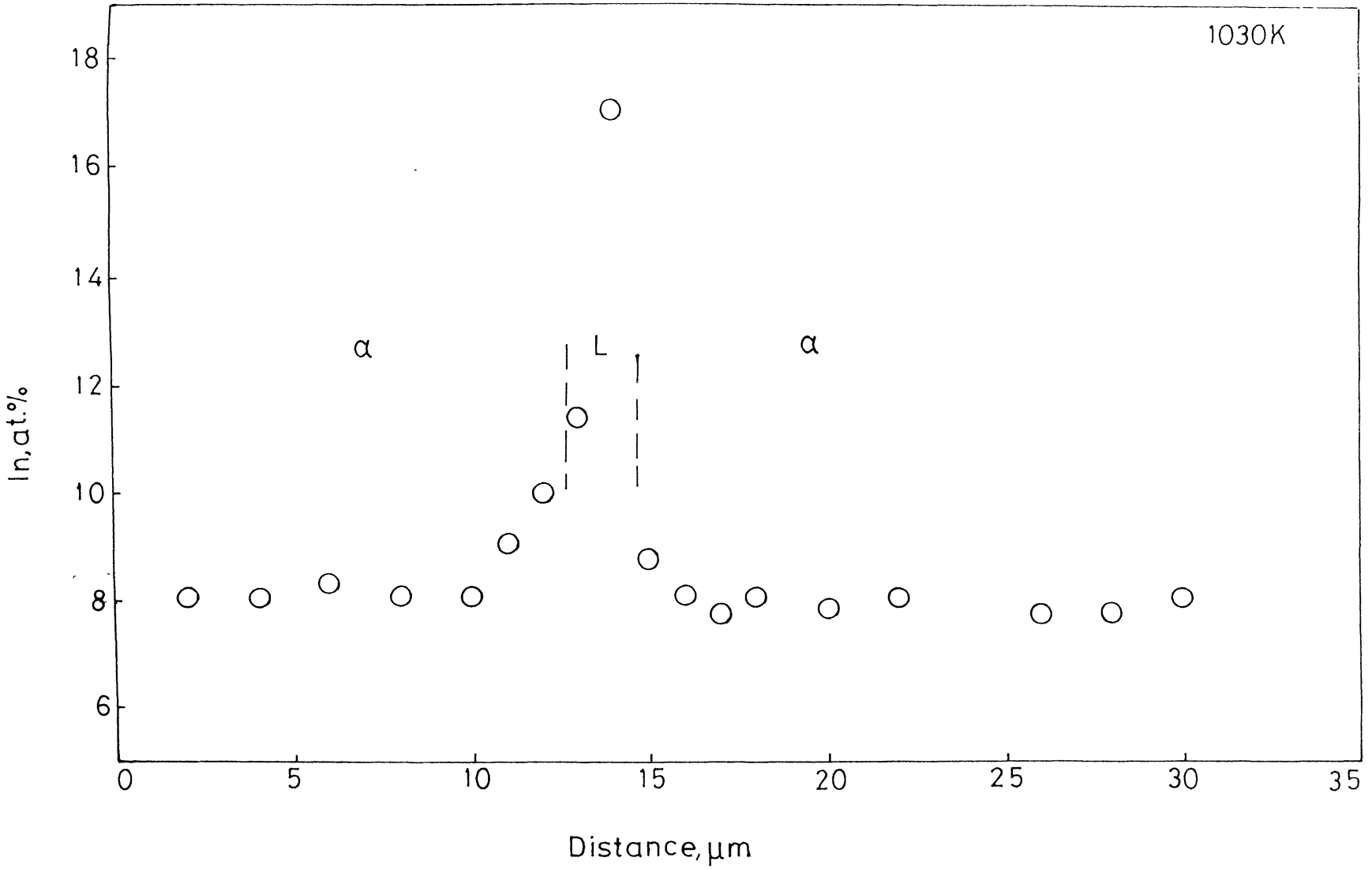

Fig. 15 c. Composition profile of In across the lamellar structure, 757°C, Cu-9.5 at.pct. In alloy.

value. This is depicted clearly in all the concentration profiles shown in Fig. 15 a, b and c. The concentration of the depleted matrix was taken as the average value of a number of readings on both sides of liquid lamellae. The concentration of the depleted matrix is shown in Fig. 16 for both alloy compositions along with the equilibrium solidus and liquidus boundaries experimentally determined by Muschik et al (21). There is a departure in composition of the depleted matrix from the equilibrium solidus for both alloy compositions. This is consistent with the results of cellular precipitation where the depleted matrix composition of solute lies to the right of the equilibrium solvus composition. The result is also consistent with the theory of the cellular precipitation after Cahn (8). The depleted matrix composition in the Cu-9.5 at.pct. In alloy departs more from the equilibrium solidus when compared with the data obtained for the Cu-8.9 at.pct. In alloy. The above results are expected due to the higher growth rate in the Cu-9.5 at.pct. In alloy.

3.5 Kinetics

Since many of the characteristics of the growth of cells during solid to liquid transformation are similar to those observed for the cellular precipitation reaction the kinetics can be described by using some of the theories of cellular precipitation.

Following Cahn's theory (8) of cellular precipitation, the differential equation can be written as

$$\frac{dX_B}{dt} = D_L \frac{d^2 X_B^L}{dx^2} + \frac{v}{\delta}({}^1X_B^\alpha - X_B^\alpha), \qquad (3.1)$$

where X_B^L, ${}^1X_B^\alpha$ *and* X_B^α are solute compositions of the liquid, original alloy and depleted matrix, respectively. It is assumed that there is no composition variation in the liquid across the liquid film thickness, δ, at the migrating interface and the coherent strain energy is negligible. The migrating interface is planar and the diffusion occurs through the thin liquid layer separating the original alloy and the depleted matrix. The diffusion coefficient of solute in the liquid is D_L. It is also assumed that the diffusivity of

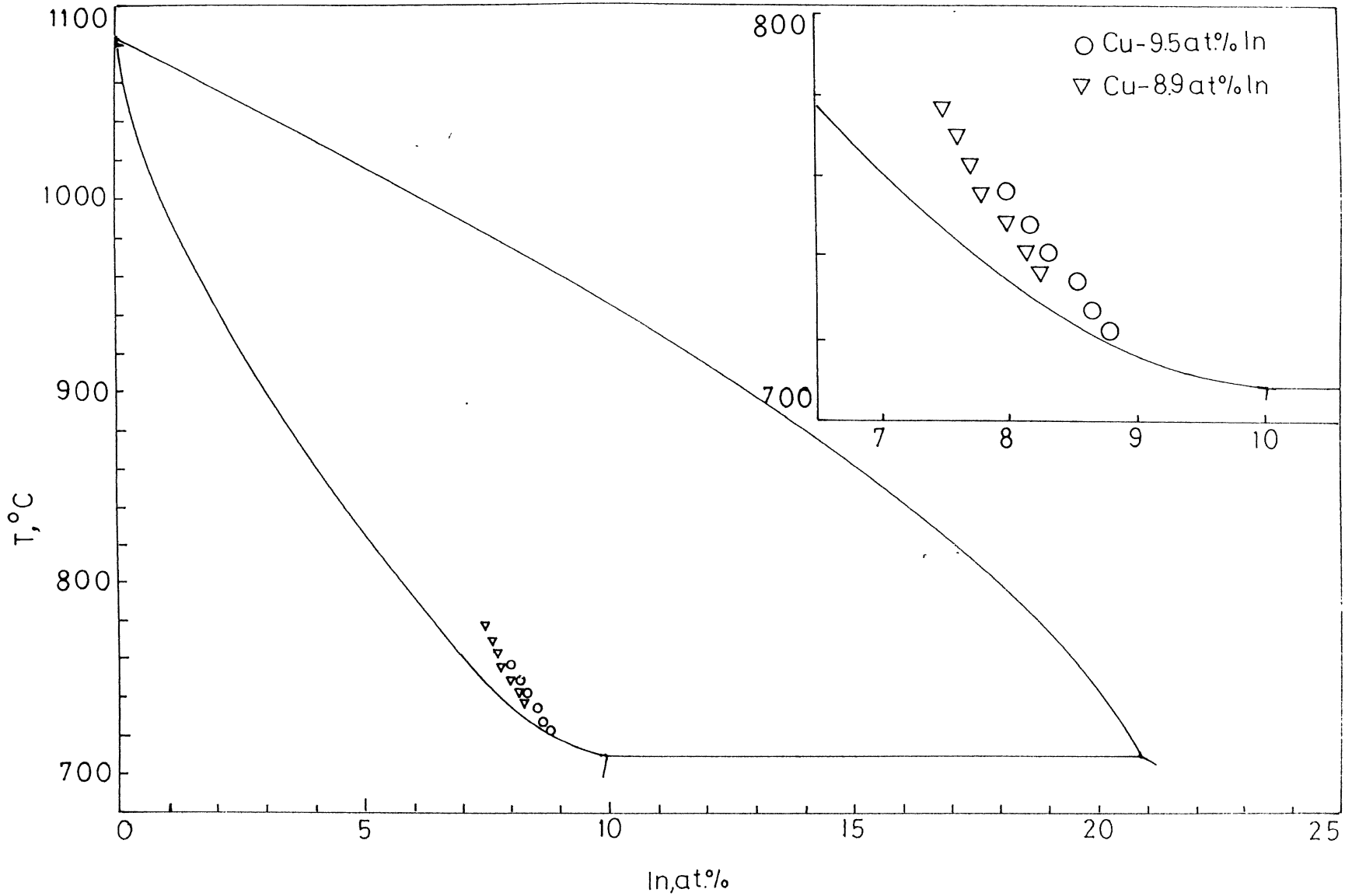

Fig. 16. Composition of the depleted matrix (α). The equilibrium solidus and liquidus lines are shown (9). The magnified view is shown in the inset.

solute in the liquid is independent of solute concentration in the range of small composition change that occurs during the reaction. The composition of solute in the liquid can be converted to the appropriate composition of the solid using the partition coefficient, k ($=X_B^\alpha / X_B^L$). Under steady state, equation (3.1) can be written as

$$\frac{D_L \delta}{k} \frac{d^2 X_B^\alpha}{dx^2} + v({}^1X_B^\alpha - X_B^\alpha) = 0. \qquad (3.2)$$

The solution of the differential equation can be obtained on the same lines as worked out by Cahn (8) for the cellular precipitation with the result

$$\alpha = \frac{k v \lambda^2}{D_L \delta}, \qquad (3.3)$$

where α can be determined from the fraction of the solute precipitated as liquid. It is related to the compositions from the relation

$$\frac{{}^1X_B^\alpha - X_B^\alpha}{{}^1X_B^\alpha - {}^eX_B^\alpha} = \frac{2}{\sqrt{\alpha}} \tanh\left(\frac{\sqrt{\alpha}}{2}\right), \qquad (3.4)$$

where ${}^eX_B^\alpha$ is the equilibrium solidus composition.

Following Turnbull's theory of cellular precipitation (18), the flux of solute rejected during growth of the α lamellae equals the flux of solute through the layer of liquid at the migrating interface. The diffusion equation can be written as

$$v({}^1X_B^\alpha - X_B^\alpha)\lambda^\alpha = -2D_L\delta \frac{\partial X_B^L}{\partial x} \cong +\frac{2D_L\delta}{k} \frac{\Delta X_B^\alpha}{\Delta x} \qquad (3.5)$$

Taking the effective diffusion distance Δx as $\lambda^\alpha/2$, which is half width of the α lamellae, the diffusivity can be written as

$$D_L\delta = \frac{k v\lambda^2 (f^\alpha)^2 ({}^1X_B^\alpha - X_B^\alpha)}{4({}^1X_B^\alpha - {}^eX_B^\alpha)}, \qquad (3.6)$$

where f^α is the fraction of the α phase in the two phase mixture and ${}^eX_B^\alpha$ is the equilibrium solidus composition. Similarly, the theory of cellular precipitation after Petermann and Hornbogen (9) can be applied to describe the kinetics of growth of the cells in the present investigation. This can written as

$$D_L\delta = \frac{-v\lambda^2 RTk}{8\Delta G}, \qquad (3.7)$$

where T is the isothermal transformation temperature in *K* and ΔG is the driving force which can be calculated from compositions and the activity data for In and Cu in solid solutions. The ΔG value can be estimated from $\Delta G=\Delta G^C-\Delta G^\gamma$, where ΔG^C is the chemical free energy change and ΔG^γ is the interfacial free energy associated with the α/Liquid interface. The ΔG^C has been calculated from, the relation,

$$\Delta G^C = RT\left[{}^1X_B^\alpha \ln \frac{a_B^\alpha}{{}^1a_B^\alpha} + {}^1X_A^\alpha \ln \frac{a_A^\alpha}{{}^1a_A^\alpha}\right] \qquad (3.8)$$

using the activity data in solid Cu-In alloys at 1000K from the work of Bhattacharya et al (23). The activity of Cu was obtained by integration of Gibbs-Duhem equation from the activity data of In in Cu-In alloys at 1000K. Since the transformation has been carried out in a small temperature interval of 40K the temperature dependence of the activity has not been considered. The solid/liquid interfacial energy of the Cu-In alloy of this investigation has not been reported in the literature. It can be estimated from those of Cu and another low melting metal Sn. The specific interfacial energy, γ_{SL} of the solid/liquid interface has been reported by Turnbull (24) to be 177 mJm^{-2} at the melting point of pure Cu. The specific interfacial energy of the solid/liquid interface of pure In at the melting point is not available, however, for another low melting metal Sn, the value has been reported (24) to be 55 mJm^{-2} at its melting point. Connecting the two interfacial

energies at their melting points gives a value of approximately 160 mJm^{-2} as the solid/liquid interfacial energy for the alloy. The interfacial free energy, ΔG^{γ} was calculated from the relation $\Delta G^{\gamma} = \frac{2\gamma_{SL}\ Vm}{\lambda}$, where V_m is the molar volume of the alloy composition which were determined from the lattice parameter data reported by Subramaniam et al (25).

The calculated values of ΔG^{C}, ΔG^{γ} and ΔG are shown in table 1 along with the growth rate, interlamellar spacing and composition data. The interfacial free energies are very small compared to ΔG^{C} and are due to an order of magnitude higher interlamellar spacings as compared to those observed during cellular precipitation reactions. The driving force available for the solid to liquid transformation in the two-phase field (α+liquid) is higher for the Cu-9.5 at.pct. In alloy as expected. These are shown in Fig. 17 as a function of temperature for the two alloy compositions studied in this investigation.

The diffusivity values, $D_L\delta$, were calculated for the above three models and the data are shown in table 2. The $\ln(D_L\delta)$ values are plotted against the reciprocal of absolute temperature in Fig. 18 a, b and c. For the model after Cahn (8), the $D_L\delta$ values lie in the range 1.3×10^{-17} to $2 \times 10^{-17} m^3s^{-1}$. Considering the liquid film thickness to be 2×10^{-7}m, the liquid diffusion coefficient, D_L, will lie close to $10^{-10} m^2s^{-1}$, which is within one order of magnitude of the liquid diffusion coefficient in most metals and alloys near their melting points. The maximum value of the diffusivity, $D_b\delta$, obtained during cellular precipitation in the Cu-8.9 at. pct. In alloy lies in the range 10^{-21} to $10^{-22} m^3s^{-1}$ using mass balance (18, 26) similar to that carried out in formulating equation (3.6). The diffusivity obtained in the present investigation therefore is four to five orders of magnitude higher than those observed for the cellular precipitation reaction where solute transport through grain boundaries controls the transformation kinetics. The $D_L\delta$ values from the mass balance also lies in the $1.5X10^{-17}$ to $2X10^{-17} m^3s^{-1}$ range.

The diffusivity, $D_L\delta$, values for the Petermann and Hornbogen analysis (9) lie in the 10^{-15} to 10^{-16} m^3s^{-1}range for both alloy compositions, which again is four to five

Table 1a: Composition , growth rate, interlamellar spacing and the free energy for the Cu-9.5 at.pct. In alloy.

Temperature (K)	X_{In}^{α} *(at. pct.)*	v *(μm/s)*	λ *(μm)*	$2\gamma V_m/\lambda$ *(J/mol)*	$-\Delta G^c$ *(J/mol)*	$-\Delta G$ *(J/mol)*
996	0.088	1.50	11.0	0.22	122.37	122.15
1001	0.0866	2.046	10.1	0.24	137.43	137.19
1008	0.0855	4.030	7.86	0.31	153.68	153.37
1015	0.083	7.772	6.22	0.4	178.47	178.07
1022	0.082	11.64	5.56	0.44	197.38	196.94
1030	0.08	16.42	4.92	0.50	211.96	211.46

Table 1b: Composition, growth rate, interlamellar spacing and the free energy for the Cu-8.9 at.pct. In alloy.

Temperature (K)	X_{In}^{α} *(at. pct.)*	v *(μm/s)*	λ *(μm)*	$2\gamma V_m/\lambda$ *(J/mol)*	$-\Delta G^c$ *(J/mol)*	$-\Delta G$ *(J/mol)*
1010	0.082	1.36	13.2	0.19	73.10	72.91
1015	0.0816	2.87	9.6	0.26	79.26	79.0
1022	0.08	5.17	7.61	0.32	89.27	88.95
1029	0.079	8.47	6.47	0.38	97.29	96.91
1036	0.077	13.3	5.47	0.45	103.88	103.43
1043	0.076	19.89	4.67	0.53	107.09	106.56
1050	0.075	25.0	4.35	0.57	109.08	108.51

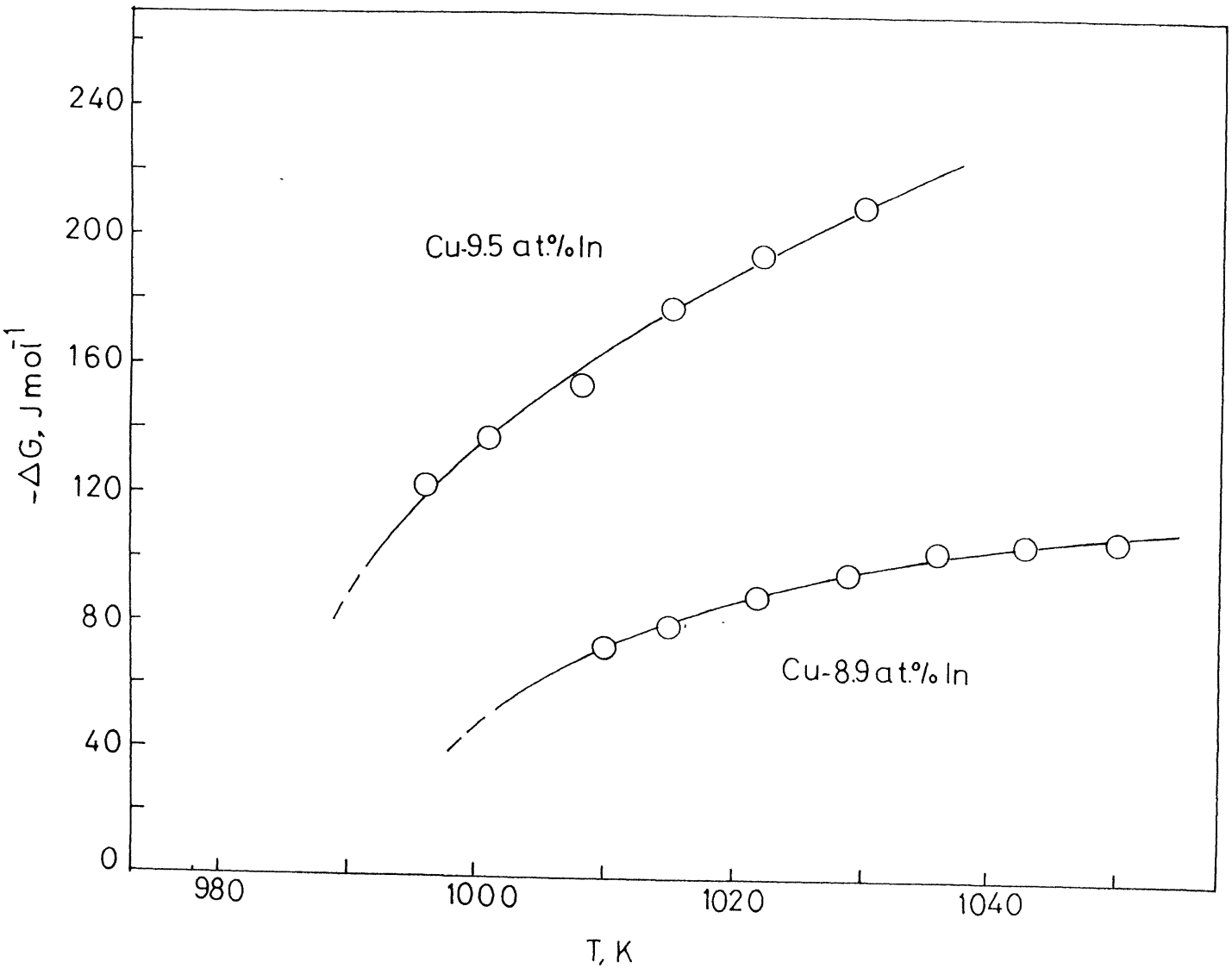

Fig. 17. Driving force as a function of temperature for the growth of the lamellar structure consisting of alternate lamellae of liquid and solid phase.

Table 2a. $D_L\delta$ values for the three models, for Cu-9.5 at.pct. In alloy.

T, K	$D_L\delta$		
	Cahn model	**Petermann and Hornbogen model**	**Mass Balance model**
996	1.556E-17	6.33611E-16	1.2078E-17
1001	1.614E-17	6.45225E-16	1.3076E-17
1008	1.696E-17	6.80487E-16	1.4540E-17
1015	1.736E-17	6.84397E-16	1.5600E-17
1022	1.819E-17	7.27968E-16	1.7110E-17
1030	1.890E-17	7.33092E-16	1.7489E-17

Table 2b. $D_L\delta$ values for the three models, for Cu-8.9 at.pct. In alloy.

T, K	$D_L\delta$		
	Cahn model	**Petermann and Hornbogen model**	**Mass Balance model**
1010	1.37764E-17	1.33844E-15	1.3839E-17
1015	1.37903E-17	1.35927E-15	1 4301E-17
1022	1.42904E-17	1.3428E-15	1 5173E-17
1029	1.51661E-17	1.43751E-15	1 6045E-17
1036	1.66689E-17	1.486E-15	1.7674E-17
1043	1.56817E-17	1.55069E-15	1.7675E-17
1050	1.60615E-17	1.63521E-15	1.8075E-17

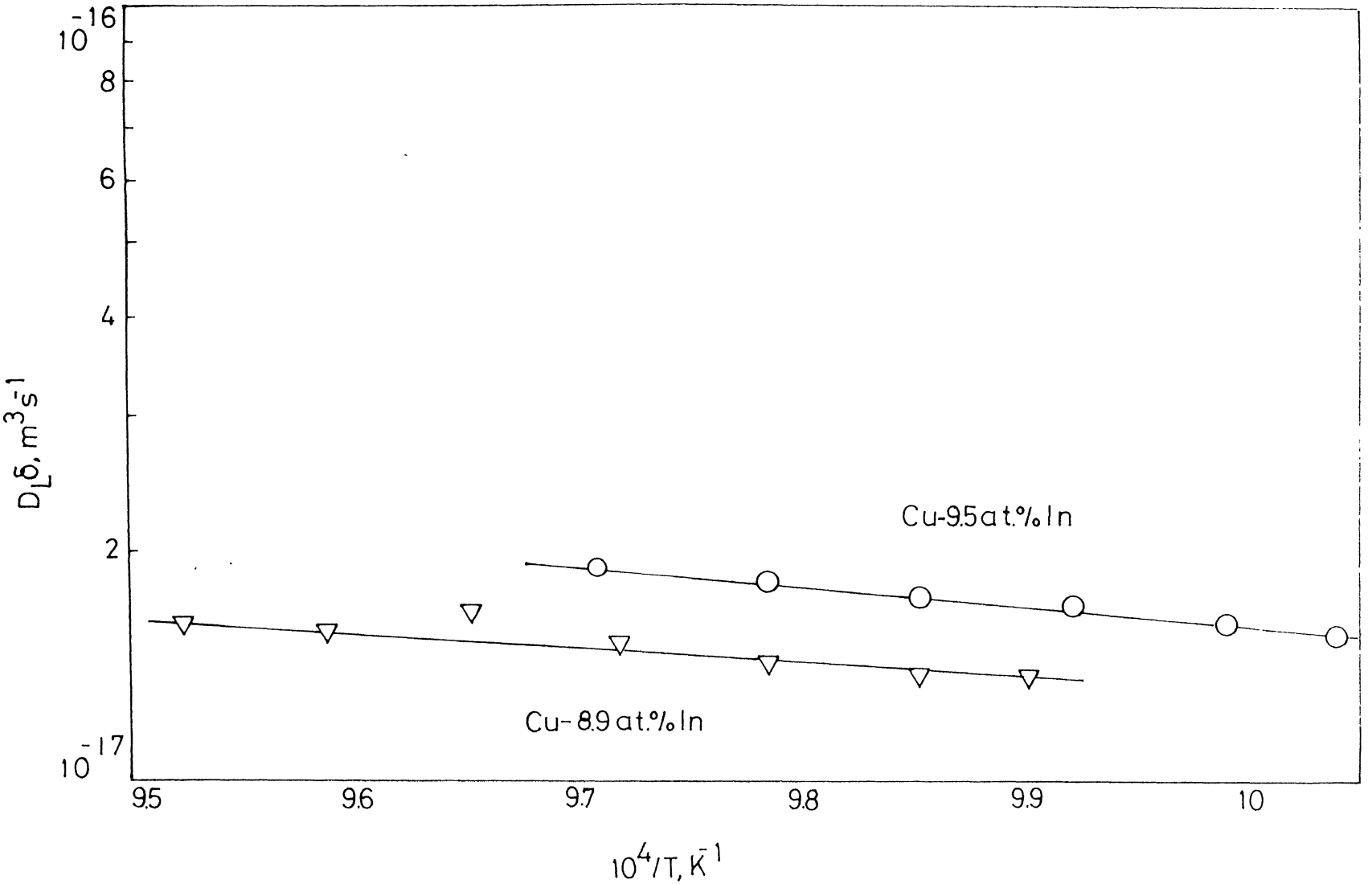

Fig. 18 a. $\ln(D_L\delta)$ vs 1/T for model after Cahn.

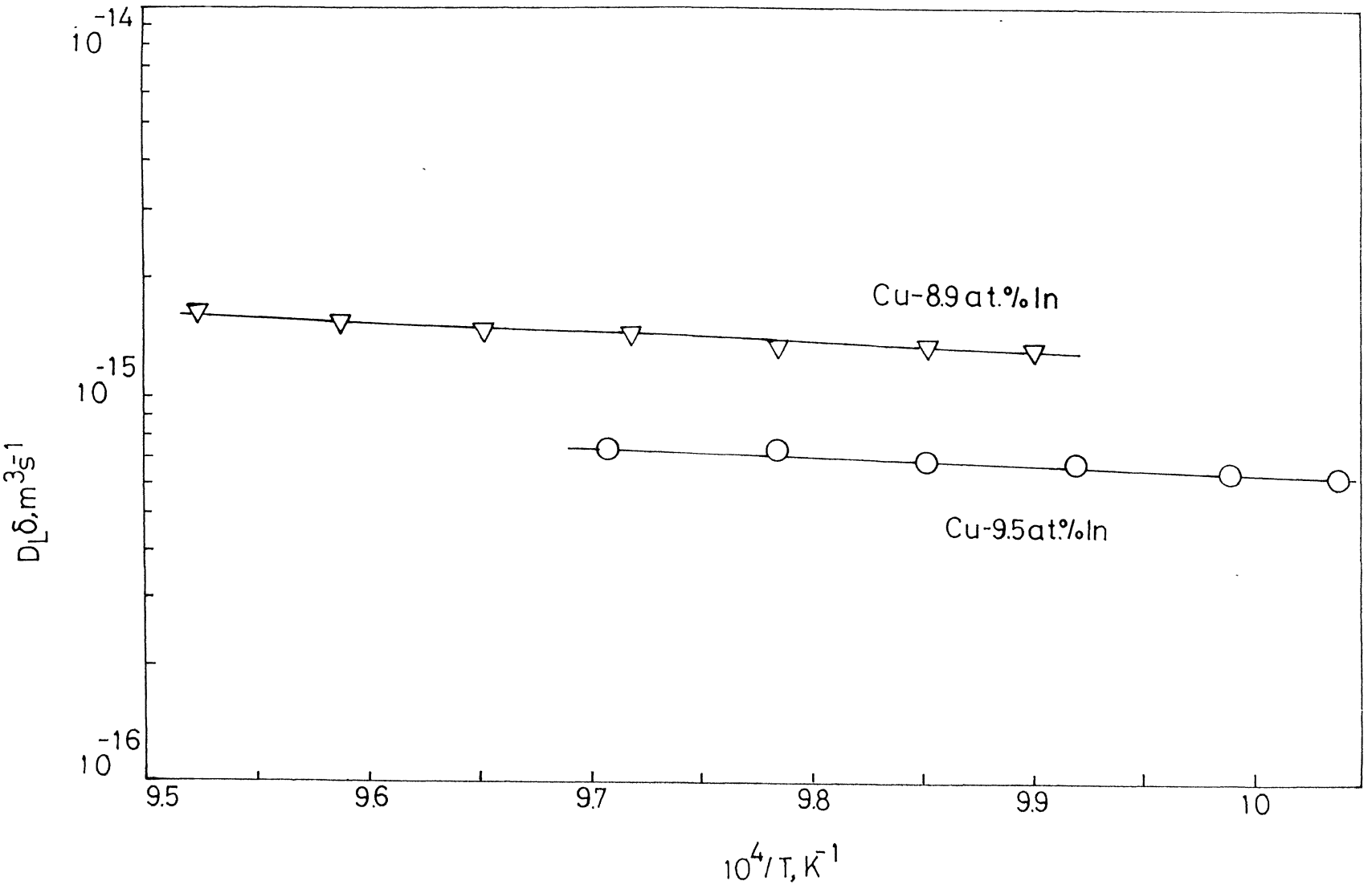

Fig. 18 b. $\ln(D_L\delta)$ vs 1/T for model after Petermann and Hornbogen.

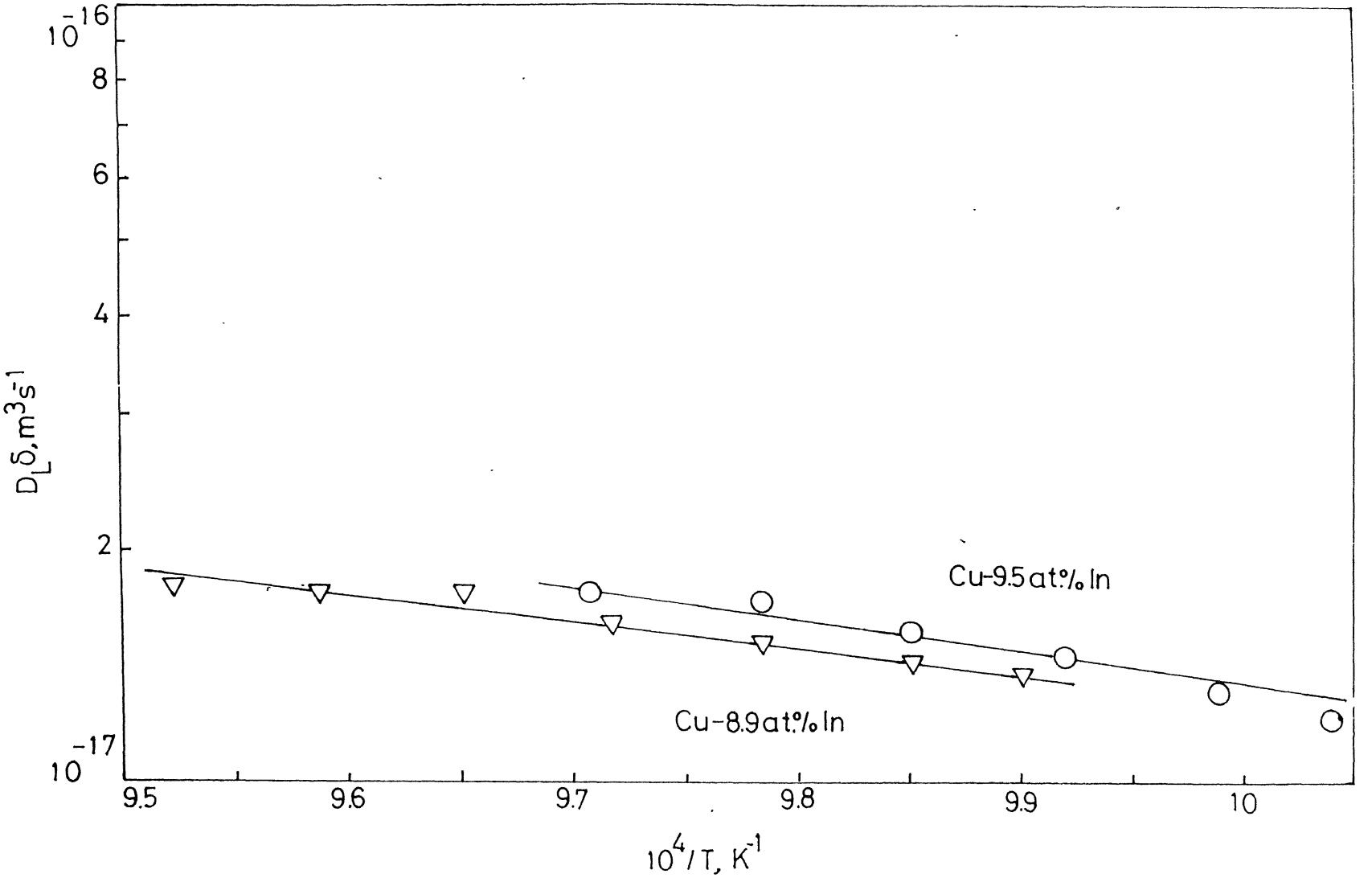

Fig. 18 c. $\ln(D_L\delta)$ vs 1/T for model using mass balance.

orders of magnitude higher than the maximum diffusivity value at 458°C (1) for the cellular precipitation reaction in the Cu-8.9 at.pct. In alloy. The diffusion coefficient in the liquid, D_L, lies in the range 10^{-8} to 10^{-9} m^2s^{-1} which agrees well with those of liquid metals at their melting points.

The average diffusion coefficient in liquid, $\overline{D_L}$, was calculated from self diffusion coefficients of liquid Cu and In and using the equation,

$$\overline{D_L} = \left(D_{L(Cu)}.X_{In} + D_{L(In)}.X_{Cu}\right).\left(1+\frac{X_{In}}{X_{Cu}}\frac{d\ln\gamma_{In}}{d\ln X_{In}}\right), \qquad (3.9)$$

where $D_{L(Cu)}$ and $D_{L(In)}$ are the self diffusion coefficients for Cu and In, respectively, in the liquid, X_{In} and X_{Cu} are the mole fractions of In and Cu respectively and γ_{In} is the activity coefficient of In in Cu-In alloys. The self diffusion coefficients of Cu and In in the liquid state were calculated from

$$D_{o(Cu)} = 14.7X10^{-8}m^2s^{-1},\ Q_{Cu} = 40.62kJmol^{-1}(27),$$
$$D_{o(In)} = 2.89X10^{-8}m^2s^{-1},\ Q_{In} = 10.16kJmol^{-1}(28).$$

The Arrehenius parameters for the calculation of D_L, self diffusion coefficients, are applicable in the temperature range 1140-1270°C for Cu and 170-750°C for In. The calculation of $\overline{D_L}$ has been made at 1000K. It is assumed that the self diffusion coefficient parameters, D_o and Q for Cu are valid at 1000K. The parameter $(d\ln\gamma_{In}/d\ln X_{In})$ was calculated from the activity coefficient versus composition data of Bhattacharya et al (23). The calculation has yielded

$$D_{L(Cu)} = 1.1X10^{-9}m^2s^{-1},\ D_{L(In)} = 8.5X10^{-9}m^2s^{-1}, \text{ and}$$

$d\ln\gamma_{In}/d\ln X_{In}$=0.05. This gives $\overline{D_L}$=$8X10^{-9}m^2s^{-1}$ at 1000K. The diffusion coefficient obtained at 1001K for the Cu-9.5 at.pct. In alloy is 10^{-10} for the Cahn's (8) model and the procedure using mass balance. For the Petermann and Hornbogen model (9), the D_L values at 1001K lie in the range of 10^{-8} to $10^{-9}m^2s^{-1}$ for the two alloy compositions.

The activation energy was calculated from the slope of the best straight line drawn through the data points. The activation energy has values of 43.8 and 36 $kJmol^{-1}$ for Cu-9.5 at.pct. In and Cu-8.9 at.pct. In alloy, respectively, when equation (3.3) after Cahn (8) was used. The activation energies for the Petermann and Hornbogen model (9) has values of 39.1 and 38.9 $kJmol^{-1}$ for the Cu-9.5 at.pct. In and Cu-8.9 at.pct. In alloys, respectively. The activation energy values obtained using simple mass balance are 63 and 61 $kJmol^{-1}$ for Cu-9.5 at.pct. In and Cu-8.9 at.pct. In alloys, respectively which are 20 to 25 $kJmol^{-1}$ higher than those obtained for the other two models.

The activation energy of self diffusion of Cu in pure solid Cu and substitutional solutes In, Sn and Sb in Cu in solid dilute alloys has been reported (28) to be 210, 190-220, 170-200 and 200 $kJmol^{-1}$, respectively. The difference between the activation energies of self diffusion of Cu in Cu and the substitutional solutes, In, Sn and Sb is very small. Considering that the behavior will be very similar in liquid Cu and liquid Cu-In alloys, the activation energies of self diffusion in liquid Cu and that of In in liquid Cu are expected to be very close. The activation energy of self diffusion in liquid copper has been reported to be 40.62 $kJmol^{-1}$ (27). The corresponding value for the diffusion of In in liquid Cu-In alloys is not available but is expected to be close to the self diffusion in liquid Cu and agrees well with the activation energy values obtained in this investigation.. The activation energy values obtained for cellular precipitation reaction in a Cu-8.9 at.pct. In alloy lie in the range 135-160 $kJmol^{-1}$, which is three to four times higher than the activation energy values obtained for the models of Cahn (8) and Petermann and Hornbogen (9). Clearly, since the cellular precipitation in Cu-In alloys occurred by solute transport along the grain boundaries, the diffusion mechanism appears to be is different during discontinuous growth of the liquid and solid lamellae in these alloys. From the activation energy values and diffusivities it can be concluded that the discontinuous growth of liquid and solid, two phase, lamellar structure occurs by solute transport through a thin liquid film formed as the migrating interface.

CHAPTER 4

CONCLUSIONS

The following conclusions can be drawn:

1. Cu-In alloys containing 8.9 and 9.5 at.pct. In decompose to a lamellar structure consisting of alternate lamellae of depleted α and liquid phases when allowed to transform in the (solid+liquid) phase field. The transformation occurs by the discontinuous precipitation of the liquid phase, which nucleated at the grain boundaries.

2. A thin liquid layer has formed between the supersaturated and depleted solid α.

3. The growth rate increased with increasing temperature of transformation. However, the interlamellar spacing was observed to decrease with the increasing transformation temperature. Both growth rates and interlamellar spacings were higher by one to three orders of magnitude when compared with the cellular precipitation in these alloys. The rate of migration of the liquid/solid interface was higher in the Cu-9.5 at.pct. In alloy as compared to Cu-8.9 at.pct. In alloy and can be correlated to the much higher driving force available for transformation in the Cu-9.5 at.pct. In alloy. The interlamellar spacing of the Cu-8.9 at.pct. In alloy was observed to be higher than those of the Cu-9.5 at.pct. In alloy at all temperature of transformation in this investigation. This can be interpreted to be due to more time available for diffusion in the Cu-8.9 at.pct. In alloy due to lower rate of growth.

4. The diffusion coefficient calculated from the growth rate, interlamellar spacing and composition data indicates that its value lies in the range 10^{-9} to 10^{-10} m^2s^{-1} at 1001K. The activation energies have been calculated to lie in the range 40 ± 5 $kJmol^{-1}$ for models after Cahn (8) and Petermann and Hornbogen (9) and a higher value in the range 61-63 $kJmol^{-1}$ from mass balance. The activation

energies are much lower than those reported for volume diffusion or for boundary diffusion in these alloys in the solid state. The diffusion coefficient and the activation energy values obtained in this investigation clearly indicate that the solute transport occurs through the thin layer of liquid formed between the transformed and untransformed regions of the matrix.

References

1. S. P. Gupta, Acta Metall. 34, 1279 (1986).
2. S. P. Gupta, Acta Metall. 35, 747 (1987).
3. R. A. Fournelle, Acta Metall. 27, 1147 (1979).
4. S. P. Gupta and G. T. Parthiban, Z. Metallk. 76, 505 (1985).
5. Y. S. Kucharenko, Izv. Akad. Nauk. SSSR, Metaly. 6, 116 (1973).
6. Y. S. Kucharenko, Fiz. Metal. Metalloved. 39, 815 (1975).
7. T. Muschik, W. A. Kaysser and T. Hehenkamp, Acta Metall. 37, 603 (1989).
8. J. W. Cahn, Acta Metall. 7, 18 (1959).
9. J. Petermann and E. Hornbogen, Z. Metallk. 59, 814 (1968).
10. H. Bohm, Z. Metallk. 52, 564 (1961).
11. G. Meyrick, Scripta Metall. 10, 649 (1976).
12. C. S. Smith, Trans. ASM, 45, 533 (1953).
13. K. N. Tu and D. Turnbull, Acta Metall. 15, 369 (1967).
14. K. A. Kamatsu, W. Gust, M. B. Hintz and B. Priedel, Solid State Transformation, 133-198.
15. R. A. Fournelle and J. B. Clark, Metall. Trans. 3, 2757 (1972).
16. K. N. Tu, Metall. Trans. 3, 2769 (1972).
17. D. Y. Yoon, Inter. Materials Reviews 40, 149 (1995).

18. D. Turnbull, Acta Metall. 3, 55 (1955).

19. E. Nes and H. Billdal, Acta Metall. 25, 1039 (1977).

20. J. Hertz, Journal of Alloys and Compounds. 321, 201 (2001).

21. T. Muschik and T. Hehenkamp, Z. Metallk. 78, 358 (1987).

22. B. E. Sundquist, Acta Metall. 16, 1413 (1968).

23. D. Bhattacharya and D. B. Masson, Metall. Trans. 5, 1357 (1974).

24. D. Turnbull, J. Appl. Phys. 21,1022 (1950).

25. P. R. Subramanium and D. E. Laughhi, Bull. Alloy. Phase Diag. 10, 554 (1989).

26. H. I. Aaronson and Y. C. Liu, Scripta Metall. 2, 1 (1968).

27. J. Henderson and L. Young, Trans. Met. Soc. AIME 221, 72 (1961).

28. A. Lodding, Z. Naturforsch. 11a, 200 (1956).

29. K. Hoshino, Y. Iijima and K. Hirano, Acta Metall. 30, 265 (1982).